Chapter N

Optical Wave Turbulence

S. K. Turitsyn, S. A. Babin, E. G. Turitsyna,
G. E. Falkovich, E. V. Podivilov, D. V. Churkin

We review recent progress in optical wave turbulence with a specific focus on the fast growing field of fibre lasers. Weak irregular nonlinear interactions between a large number of resonator modes are responsible for practically important characteristics of fibre lasers such as spectral broadening of radiation. Wave turbulence is a fundamental nonlinear phenomenon which occurs in a variety of nonlinear wave-bearing physical systems. The experimental impediments and the computationally intensive nature of simulating of hydrodynamic or plasma wave turbulence often make it rather challenging to collect a significant number of statistical data The study of turbulent wave behaviour in optical devices offers quite a unique opportunity to collect an enormous amount of data on statistical properties of wave turbulence using high-speed, high precision optical measurements during a relatively short period of time. We present recent theoretical, numerical and experimental results on optical wave turbulence in fibre lasers ranging from weak to strong developed turbulence for different signs of fibre dispersion. Furthermore, we report on our studies of spectral wave condensate in fibre lasers that make interdisciplinary links with a number of other research fields.

Chapter contents

N.1 Optical Wave Turbulence: Introduction

Wave turbulence is a fundamental nonlinear phenomenon that occurs in a variety of nonlinear physical systems (see e.g. [Zakharov *et al.*, 1992, S. Nazarenko, 2011] and references therein). Turbulence is a state of system with many degrees of freedom deviated far away from equilibrium. Even when an external excitation only effectively acts on one or a few waves, nonlinear interactions between waves lead to excitation of many waves and turbulence. Wave turbulence theory deals with the statistical behaviour of a large number of interacting waves. Turbulence theory is one of the most challenging and truly fundamental theoretical problems with applications ranging from turbulent combustion

in engines to turbulent effects in atmosphere and in outer space [Frisch, 1995, Falkovich, 2006; Falkovich and Sreenivasan, 2006]. There are two primary types of physical systems with turbulent-like behaviour. First case, mostly associated with using the term *turbulence*, is the so-called "fully developed wave turbulence" when scales, where waves are excited (energy is pumped into the system) are well separated from the scales where waves are dissipated. In this instance the turbulent energy transfer between spectral components in the inertial interval does not depend heavily on the details of excitation and dissipation [Zakharov *et al.*, 1992]. In the second case, the scales at which energy is pumped into the system and disappeared cannot be fully separated and turbulence does not have a well-defined inertial interval. In this Chapter we present a rather interesting and important example of nonlinear optical systems, - fibre lasers – which exhibit wave turbulence behaviour of the second type.

The term *optical turbulence* is used in literature in a variety of rather different research contexts. For instance, optical turbulence is often referred to as an atmospheric effect caused by fluctuations of the refractive index in the air that affects the propagation of light beams. This effect can significantly degrade infrared images or bit error rates in free-space lasers and ground-to-satellite communication systems and is one of the main causes that limit the spatial resolution attainable in ground-based astronomical long-range imaging systems. Optical turbulence has also been studied in experiments with a ring resonator synchronously driven by a train of pico-second light pulses [Mitschke *et al.*, 1996]. Chaotic behaviour of pulses resulted from nonlinear interactions and repetitive interference of a train. Furthermore, intra-pulse correlations have been used as a measure of the degree of complexity of generated temporal and spatio-temporal chaos and turbulence [Mitschke *et al.*, 1996]. An interesting example of turbulent-like behaviour of optical waves can be found in semiconductor lasers with delayed feedback. The latter is described by a generalized complex Swift-Hohenberg equation [Lega *et al.*, 1995] which is broadly used as a generic model in studies of filamentation in wide aperture lasers and pattern formation in the transverse section of semiconductor lasers. Finally, very important theoretical studies of optical turbulence have been undertaken in the general context of the chaotic behaviour of system solutions of nonlinear

partial differential equations. The turbulence associated with the so-called nonlinear Schrodinger equation (NLSE) is often called optical turbulence because of its relevance to the propagation of light beams in transparent media with a nonlinear refractive index. In particular, in the frameworks of the 2D NLSE model [Dyachenko *et al.,* 1992*;* Newell *et al.,* 2001, Zakharov *et al.,* 2004; Dyachenko and Falkovich, 1996; Zakharov and Nazarenko, 2005] studies have focused on the so-called fully developed wave turbulence in which the number of active degrees of freedom is very large (corresponding in hydrodynamics to the large Reynolds number limit). Since NLSE has two integrals of motion, it allows for two cascades: a direct cascade of energy towards small scales and an inverse cascade of wave action (number of waves) towards large scales. An inverse cascade is arguably the most conceptually novel idea in turbulence since Kolmogorov. In a finite system, an inverse cascade leads to the creation of the spectral condensate i.e. the mode coherent across the whole system. In wave systems like NLSE, condensate corresponds to a monochromatic wave. One then distinguishes cases with a stable and unstable condensate (NLSE with repulsion or attraction respectively). Using the focusing (attracting potential) 2D NLSE model it has been shown that wave collapse might act as a mechanism for intermittency and a statistical behaviour, which violates many of the traditional assumptions made by Kolmogorov [Kolmogorov, 1941; Lushnikov and Vadimirova, 2010]. On the other hand, not much is known about the interaction of stable condensate and turbulence, the system that curiously has some quantum-like feature since it combines coherence and fluctuations. Particularly, not much is known on how turbulence appears in a system where a coherent state is linearly stable (very much like fluid turbulence in pipe and channels, where laminar flows are linearly stable) This is still a topic of active research despite having over 100 year history.. We shall see below that optical turbulence in fibre lasers sheds some light on such general problems of turbulence.

Optical manifestations of turbulence [Dyachenko *et al.,* 1992*;* Newell *et al.,* 2001*;*Zakharov *et al.,*2004; Dyachenko and Falkovich, 1996; Zakharov and Nazarenko, 2005; Solli *et al.,* 2007; Falkovich *et al.,* 1996, 2001; Babin *et al.,* 2007a] are very closely linked to nonlinear optical phenomena such as self-phase and cross-phase modulation, self-focusing,

four-wave-mixing, optical soliton radiation and interactions, nonlinear spectral broadening, supercontinuum generation and optical wave breaking (see e.g. [Agrawal, 1995; Skryabin *et al.,* 2007; Dudley *et al.,* 2006; Smirnov *et al.,* 2006] and references therein). A variety of nonlinear optical effects and precision of optical experiments provide a great, but not yet fully explored potential for the study of turbulence properties through manifestations in optical problems and devices.

The main focus of this Chapter is on our recent studies of a new type of optical wave turbulence that occurs in the context of fibre Raman lasers with cavities ranging from tens of metres to hundreds of kilometres. Raman fibre lasers are stable and efficient light sources that have attracted a great deal of interest in recent years both because of its winning technical characteristics and as an important example of a nonlinear photonic device utilising nonlinear science concepts. It has been demonstrated recently that multiple four-wave-mixing (FWM) interactions between very large numbers of cavity modes are primarily responsible for practical characteristics of Raman fibre lasers, in particular, intensity fluctuations and spectral broadening of the generated radiation. These multiple interactions lead to strong de-phasing of modes and the randomization of dynamics. This process can be analyzed using the set of deterministic nonlinear ordinary differential equations describing the dynamics of modes, which are randomised due to FWM nonlinear processes. Mathematically, FWM interactions involve a huge number of rapidly oscillating terms with different amplitudes and phases making time evolution of any particular cavity mode extremely stochastic. Even weak nonlinear FWM interactions lead to a random energy exchange between waves and to de-phasing because of a continuum of modes involved in nonlinear interactions. Optical wave dynamics in powerful fibre lasers is an interesting manifestation of a physical system where long term average properties of the system are determined by a random behaviour of a huge number of weakly interacting waves - *wave turbulence.* Therefore, theoretical analysis of the spectrum formation and fluctuations requires the use of statistical techniques and approaches instead of the dynamical formalism commonly used in fibre optics. In this Chapter we will overview recent

developments in this field with a clear interdisciplinary link between fibre optics and the theory of turbulence.

N.2 Basics of Fibre Lasers

A powerful fibre laser presents both an interesting nonlinear physical system and a photonic device with an incredible range of practical applications (in telecommunications, medicine, metrology, spectroscopy, sensing, industrial cutting, welding and others). The Raman fibre laser exploits the effect of simulated Raman scattering (SRS). In the process of SRS, a pump photon gives up its energy to create a new photon at a longer wavelength, plus some residual energy, which is absorbed by the fibre material in the form of optical phonons. In contrast to bulk media where the light beam should be focused tightly into the substrate to observe the effect, the optical fibres that allow high-intensity light propagation over long distances, provide a much stronger SRS effect. More specifically, very low absorption of light (α~0.2 dB/km at the wavelength λ~1.55 μm corresponding to the transparency window of silica glasses) and small fibre core diameter (5-10 μm) result in the propagation of high intensity light without significant attenuation, thus providing homogeneous intensity distribution in kilometer-scale fibre spans. At the same time, the SRS of the high-intensity wave treated as a pump, induces Raman amplification of the red-shifted Stokes wave with a coefficient ~1 dB/(kmW) that becomes much higher than its attenuation already at relatively low power, ~1 W. In a conventional single mode fibre (SMF) with a germanium doped silica core, the Raman gain spectrum is rather broad with a maximum shift by ~ 14 THz at the Stokes wavelength from the pump wavelength. The Raman gain medium may be placed in a cavity, which is typically formed by the insertion of two fibre Bragg gratings (FBGs) at each end of the fibre, playing the role of "mirrors" and trapping photons within the grating bandwidth, resonantly reflecting the forward and backward propagating Stokes waves. As a result, it is possible to achieve lasing in a fibre waveguide with the cavity length L to the order of several kilometres [Grubb *et al.*, 1995]. Several frequency conversion cascades based on Stokes lines resonating in nested

cavities shift the pump power deep into the longer wavelength region. Based on the Raman gain medium and cavity FBGs reflecting specific wavelengths, Raman fibre lasers (RFLs) involving single- as well as multiple-order Stokes shifts can be designed to operate at almost any wavelength in the near-IR region (1.1-1.7 micron) pumped by high-power lasers at ~1.06 micron, e.g. by Yb-doped fibre laser providing all-fibre design. Furthermore, the number of conversion stages from short to long-wavelength edge may be reduced using as a Raman media P_2O_5-doped silica fibres with 3-times larger Stokes shift [Dianov *et al.*, 1997]. RFLs present excellent candidates for a variety of applications due to their unique attributes combining the wavelength tunability and the multi-wavelength operation [Mermelstein *et al.*, 2001] with the compactness and high power continuous wave (CW) laser diode pumps.

Of a particular interest is the ability to fully cover the spectral region near telecommunication windows of transparency, making Raman fibre lasers very attractive pump sources for distributed Raman amplification. This is considered to be one of the most important enabling technologies in high-speed optical communication [Stolen and Ippen, 1973; Mollenauer *et al.*, 1986, Chernikov *et al.*, 1999, Vasilyev, 2003, Headley and Agrawal, 2004]. Recently, an interesting realization of a first-order Raman amplified communication system providing a quasi-lossless signal transmission based on the ultra-long Raman laser architecture has been proposed and implemented (see e.g. [Ania-Castañón *et al.*, 2006] and references therein). In this particular laser, the combined forward- and backward- propagating wave generated at the Stokes wavelength (~1455 nm) inside the RFL cavity (formed in the transmission SMF fibre itself) experiences reduced variations along the fibre span. Hence, the generated intra-cavity RFL power can be used as a homogeneous, stable secondary pump to provide a near constant (along the fibre) Raman gain for optical signal transmitted at 1550 nm. If the gain is nearly equal to optical loss, a quasi-lossless transmission is possible. The quasi-lossless fibre span can be implemented using symmetric second-order pumping schemes leading to the concept of ultra-long fibre lasers [Ania-Castañón *et al.*, 2006, Ellingham *et al.*, 2006, Babin *et al.*, 2007b, Turitsyn *et al.*, 2009], which promise new applications in transmission and secure communication [Scheuer and Yariv, 2006]. Evidently, such a significant

lengthening of the RFL cavity compared to that in usual lasers leads to a new interesting class of lasers with potentially different physical mechanisms underlying their operation. Raman fibre lasers are also attractive continuous light sources for optical coherence tomography [Hsiung *et al.*, 2004], long distance remote sensing [Han *et al.*, 2005, Frazao *et al.*, 2009, Juarez *et al*, 2005], efficient excitation of a mesospheric sodium laser guide star [Huang *et al.*, 2003] and other applications (see e.g. [Kim, 2008]). Despite existing and emerging practical applications of such lasers, some fundamental physical phenomena underlying their operation and nonlinear mechanisms determining properties of generated radiation are not yet fully understood.

We will present experimental and numerical analysis of spectral and temporal characteristics of both normal scale (several km) and ultra-long Raman fibre lasers with cavity length varied from 5 km to a record laser cavity length of 270 km. We will demonstrate that important characteristics of fibre lasers are determined by turbulent-like interactions of laser modes, whose number varies for considered cavity lengths between 1 and 100 million.

N.3 Key Mathematical Models

In this section we introduce basic mathematical models focusing on the generic features of CW fibre lasers rather than on particular properties of any specific systems. Without loss of generality in what follows, we mostly consider the Raman fibre laser schemes close to the one described in [Ania-Castañón *et al.*, 2006] which provides rather uniform spatial distribution of generated Stokes waves power along the cavity formed by FBGs. However, we would like to stress that most of our approaches and methods are also applied to a much broader and fundamental class of *CW lasers with a Fabry-Perot resonator.* In numerical simulations we will use both the mathematical model, based on the standard evolution equation for the longitudinal modes (E_n) of the envelope that can be derived from the generalized Schrödinger equations for backward and forward Stokes waves with amplitudes A^+, A^- [Babin *et al.*,2006; Babin *et*

al., 2007a] and direct modelling of the amplitude equations. The slow varying part (in the direction of propagation *z* and time *t*) of amplitude of the electromagnetic field E in the cavity of length L with reflecting boundary conditions can be represented as the sum of co- and counter-propagating waves:

$$E(z,t)=\frac{1}{\sqrt{2}}\{A^{+}(z,t)e^{i(\omega_0 t-\beta_0 z)}+A^{-}(z,t)e^{i(\omega_0 t+\beta_0 z)}+c.c.\},$$

where $A^{\pm}$ corresponds to the forward and backward wave, respectively, propagating along the z-axis of the fibre, $\omega_0=2\pi c/\lambda_0$ is the frequency of the lasing (in the case of a Raman fibre laser, typically defined by the central wavelength λ_0 of the reflectors- reflection maximum), the propagation constant $\beta(\omega)$ in the medium (e.g. fibre) of the spectral components of the modulated wave whose frequency slightly deviates from a carrier frequency ω_0 can be presented as: $\beta(\omega)=\beta_0+\beta_1(\omega-\omega_0)++0.5\times\beta_2(\omega-\omega_0)^2+...$, c is the speed of light in a vacuum. We can define the total average intra-cavity Stokes wave power P (note that field intensity I in optical fibre is related to power P through the relation $P=I\,A_{eff}$, where A_{eff} is a characteristic effective area near the fibre core, where most of power is localized in direction transversal to the z-propagation) as:

$$P(z)=P^{+}(z)+P^{-}(z)=<|A^{+}|^2>+<|A^{-}|^2>. \qquad \text{(N.3.1)}$$

The evolution of $A^{\pm}$ is governed by the equations (see e.g. [Agrawal, 1995] for more details):

$$\frac{1}{v_g}\frac{\partial A^{+}}{\partial t}+\frac{\partial A^{+}}{\partial z}=\frac{1}{2}(g(P)+i\beta_2\frac{\partial^2}{\partial t^2})A^{+}-i\gamma A^{+}\left(|A^{+}|^2+2|A^{-}|^2\right) \quad \text{(N.3.2)}$$

$$\frac{1}{v_g}\frac{\partial A^{-}}{\partial t}-\frac{\partial A^{-}}{\partial z}=\frac{1}{2}(g(P)+i\beta_2\frac{\partial^2}{\partial t^2})A^{-}-i\gamma A^{-}\left(|A^{-}|^2+2|A^{+}|^2\right) \quad \text{(N.3.3)}$$

Here $v_g = 1/\beta_1$ is the group velocity, and the terms in the right-hand-side of these equations describe the following respectively: amplification/loss saturated with growth of power, dispersion and nonlinear interactions due to Kerr nonlinearity (self-phase modulation and cross-phase modulation); γ is the Kerr nonlinearity coefficient, β_2 is the fibre group velocity dispersion. Note that a more accurate model should include nonlinear terms responsible for the Raman effects and also evolution of optical fields at other wavelengths interacting with the considered waves through the Raman terms. However, here the key effect resulting from the Raman power exchange between spectrally separated waves is included through the effective gain (e.g. gain minus distributed loss) coefficient $g(P)$. Also the nonlinear coefficient γ includes the well known contribution [Agrawal, 1995] from the Raman effect leading to small renormalization of the Kerr constant. The gain $g(P)$ is a positive function at small powers and is saturated with growing power approaching zero level and, thus, defining the power level of the generated radiation P.

These equations are considered in a resonator (laser cavity) of length *L*. Boundary conditions to Eqs. (N.3.2-3) correspond to reflectors at z = 0 and z = L forming a Fabry-Perot resonator. In the spectral domain the boundary conditions defined by the point reflectors (mirrors) at the edges of cavity read:

$$A^+(0,\omega) = r_0(\omega)\, A^-(0,\omega), \;\; A^-(L,\omega) = r_L(\omega)\, A^+(L,\omega),$$

the power reflection coefficients are defined as: $R_{0,L}(\omega) = \mid r_{0,L}(\omega) \mid^2$.

Considering single round trip changes to be small, forward and backward propagating fields can be expanded in the resonator mode basis as:

$$\begin{aligned} A^+(z,t) &= \frac{1}{\sqrt{2}} \sum_{-M/2}^{M/2} E_m(t) \exp[im(\Delta t - \pi\, z / L) + \tilde{\delta}_m z / (4L)] \\ A^-(z,t) &= \frac{1}{\sqrt{2}} \sum_{-M/2}^{M/2} E_m(t) \exp[im(\pi\, z / L + \Delta t) - \tilde{\delta}_m z / (4L)] \end{aligned} \qquad \text{(N.3.5)}$$

here $\Delta = \pi\, c/(n_g L)$ is the frequency spectral mode separation, and an effective spectral dependent distributed loss is introduced as

$\tilde{\delta}_m = -\ln\ R_0(m\Delta)R_L(m\Delta)]$. Note that the phase changes introduced by the reflectors can be important in some problems [Dalloz et al., 2010]. Whilst for the sake of clarity these are not considered here, however, this effect can be easily included in a similar manner. After straightforward manipulation, the standard slow evolution (over one round trip) equation for the longitudinal mth mode can be derived:

$$\frac{\tau_{rt}}{L}\frac{dE_m}{dt} = \left(G_m - i\beta_2\Omega_m^2\right)E_m - i\gamma\sum_{i,k}E_iE_kE_{i+k-m}^* \qquad \text{(N.3.6)}$$

Here the round-trip time is $\tau_{rt} = 2Ln_g / c$ (n_g is the refractive group index). The terms on the right hand side describe, respectively, a combined effect of distributed gain and loss, and spectrally dependent loss induced by point-action reflectors at the edges of the resonator, $G_m = g - \tilde{\delta}_m / (2L)$, which is a decreasing function of the total generated power, the dispersion, $\beta_2\Omega_m^2 = \beta_2(m\,\Delta)^2$, and nonlinear terms (accounting for self-phase modulation, cross-phase modulation and four-wave mixing) induced by the Kerr nonlinearity (γ).

Note that in a dissipative (with gain and loss) physical system such as a laser, not all linear resonator modes survive competition. First, only spectral modes with mode gain overcoming the loss are amplified. Next, the modes that are amplified more than others in field dynamics might dominate the building of the radiation due to saturation of gain in other modes. The number of modes generated in laser can be approximately estimated as B_L/Δ where B_L is the laser linewidth that is related to effects limiting the spectral interval over which laser radiation is generated (e.g. fibre Bragg gratings – however, their bandwidth should be used only as an estimate of the linewidth B_L since it can depend on the total generated power). Taking that the spectral separation of modes is $\Delta \sim L^{-1}$, the number of generated modes can be very large in *long fibre lasers* (up to 100 million) making them an ideal test-bed for studies of physics far removed from the equilibrium of using one-dimensional wave turbulence.

N.4 Weak Optical Wave Turbulence in Fibre Lasers

Having a very large number of cavity modes in fibre lasers under the condition of a finite total power results in a very small amplitude of each mode. Nevertheless, experiments show that nonlinear effects are important in the considered laser systems. Thus, very weak interactions of small amplitude waves produce an observable overall effect, thus it is natural to start with a general kinetic approach already developed in a theory of weak wave turbulence [Zakharov *et al.*, 1992]. Therefore, first of all, we present a detailed analytical self-consistent theory based on wave kinetic equations. This theory describes the generation spectrum and output power of a Raman fibre laser (RFL). As we will show both theoretically and experimentally, the quasi-degenerate four-wave mixing (FWM) between different longitudinal modes is the main broadening mechanism in the RFL at high powers. We present examples of laser systems, in which the shape and power dependence of the intra-cavity Stokes wave spectrum are in excellent quantitative agreement with predictions of the theory. FWM-induced stochasticity of the amplitude and the phase of each of $\sim 10^6$ longitudinal modes generated in a RFL cavity is an example of light wave turbulence in a fibre.

N.4.1 Theory of weak wave turbulence in the context of fibre laser

In the case of the Raman fibre laser the gain/loss coefficients (N.3.2-3) take a specific form, e.g. for the Stokes wave an effective gain g depends on the averaged (over the fibre length) pump power $\overline{P}_p$ and the distributed loss as:

$$g = g_R \overline{P}_p - \alpha. \qquad \text{(N.4.1)}$$

Here $\alpha[km^{-1}]$ is the distributed loss; $g_R[W^{-1}km^{-1}]$ is the Raman gain coefficient in the optical fibre, and the average pump power $\overline{P}_p$ can be approximately expressed through the generated Stokes power P (see [Babin *et al.*, 2003] for the details) as:

$$\bar{P}_p = P_p(0)\frac{1-\exp\left(-\alpha_p L-\frac{\lambda}{\lambda_p}g_R LP\right)}{(\alpha_p+\frac{\lambda}{\lambda_p}g_R P)L}, \qquad \text{(N.4.2)}$$

here $P_p(0)$ is the input (referring to theRFL) pump power, P is the generated Stokes wave power averaged over time and the fibre cavity; α_p is the pump wave optical losses in the fibre, λ_p and λ are the pump and Stokes wavelengths, respectively. Because the RFL has a high-Q cavity, we can represent the Stokes wave as the sum of longitudinal cavity modes[similar to (N.3.5)]:

$$A^{\pm}(z,t)=\frac{1}{\sqrt{2}}\sum_m E_m(t)\exp\left(im\Delta t\mp i\kappa zm\pm\tilde{\delta}_m z/(4L)\right)\exp(-i\nu_m t), \text{ (N.4.3)}$$

where $\Delta = 2\pi/\tau_{rt}$ is the frequency spacing between adjacent Stokes wave longitudinal modes, $\tau_{rt}=2Ln_g/c$ is the RFL cavity round-trip time for the Stokes wave and $\kappa=\pi/L$. The only difference to (N.3.5) here is an explicit introduction of $\nu_m=\beta_2 v_g(m\Delta)^2/2+\gamma v_g P$ - a small frequency shift that takes into account the dispersion and the mean nonlinear phase shift. The factor $1/\sqrt{2}$ is chosen in order to normalize the total power in m-th longitudinal mode to $P_m=|E_m|^2=P_m^+ + P_m^-$.

It is convenient to rewrite the generalized nonlinear Schrödinger equation (N.3.6) for the amplitude E_m of m-th longitudinal modes in a slightly different form, which is more suitable for further manipulations:

$$\tau_{rt}\frac{dE_m}{dt}-[g(P)L-\tilde{\delta}_m/2]E_m(t)= \qquad \text{(N.4.4)}$$

$$=-i\gamma L\sum_{l\neq 0}E_{m-l}(t)\sum_{k\neq 0}E_{m-k}(t)E^*_{m-k-l}(t)\exp\left(i\beta_2 kl\Delta^2 v_g t\right),$$

where we have taken into account the effective cavity mirror losses $\tilde{\delta}_m=-\ln\left[R_1(\Omega_m)R_2(\Omega_m)\right]$ for the m-th longitudinal mode that is generated at the frequency detuned by $\Omega_m=m\Delta$ from the cavity mirror center frequency.

The right hand side (RHS) of Eq. (N.4.4) for the specific RFL cavity length of 370m considered in the experiment contains $\sim 10^{12}$ (even more in longer lasers!) different terms with random amplitudes and phases in each term that lead to a stochastic (turbulent) evolution in time (over many round trips) of the amplitude and phase of the longitudinal mode E_m. It is obvious that such an extremely complex nonlinear evolution can be described neither analytically nor numerically. For an adequate description of the Stokes wave spectrum one has to use statistical analysis. The simplest form of such analysis is based on the wave kinetic equations for the spectral power density rather than on the dynamic consideration based on deterministic equations for the multitude of longitudinal modes amplitudes E_n. Toward this end, we follow the methods of the weak wave turbulence introduced by [Zakharov *et al*, 1992].

The approach is valid in the case of small nonlinearity and this smallness condition will be quantified below. To derive from Eq. (N.4.4) the simplified wave kinetic equation for the average time-independent Stokes wave spectrum $P(\Omega)$, let us multiply Eq. (N.4.4) by E_m^* and take the real part of the expression. As a result, one can obtain the equation describing small changes of the power of the *m*-th longitudinal mode of the Stokes wave:

$$\tau_{rt}\frac{dP_m}{dt} - (2g(P)L - \tilde{\delta}_m)P_m(t) = \qquad \text{(N.4.5)}$$

$$= -Re\Big[i2\gamma L \sum_{l\neq 0, k\neq 0} E_{m-l}(t)E_{m-k}(t)E^*_{m-k-l}(t)E^*_m(t)\exp\left(i\beta_2 kl\Delta^2 v_g t\right)\Big].$$

Assuming that the phases of different longitudinal modes are random (uncorrelated), averaging the RHS of Eq. (N.4.5) in the main order leads to mean zero value as all terms include a random phase difference. In order to take into account a phase correlation induced by the FWM processes, we consider the following standard approach [Zakharov *et al*, 1992] . Instead of reproducing with full details the standard steps described in the book [Zakharov *et al*, 1992] we only outline here the

procedure and present the results. First, we find the correction to E_m by integrating the RHS of Eq. (N.4.4):

$$\delta E_m(t) = \tag{N.4.6}$$

$$= -i\gamma L \int_{-\infty}^{t} \sum_{l'\neq 0, k'\neq 0} E_{m-l'}(t') E_{m-k'}(t') E^*_{m-k'-l'}(t') \exp\left[i\beta_2 k' l' \Delta^2 v_g t'\right) \frac{dt'}{\tau_{rt}}.$$

Second, we substitute this correction (with the index *m* changed to *m-l*) for E_{m-l} in the RHS of Eq. (N.4.5), then for E_{m-k} and so on. As a result, we obtain a rather cumbersome expression, and after averaging it over a huge number of spectral components ($\sim 10^4$ in the case of the reference experiment that will be described below) near the frequency $\Omega = m\Delta$, we derive a wave kinetic equation for the stationary Stokes wave spectrum $P(\Omega) = \langle P_m \rangle / \Delta$:

$$\tau_{rt} \frac{dP(\Omega)}{dt} = [2gL - \delta(\Omega)]P(\Omega) + S_{FWM}(\Omega), \tag{N.4.7}$$

where FWM-induced terms are

$$S_{FWM}(\Omega) = \tag{N.4.8}$$

$$= -\delta_{NL} P(\Omega) + (2\gamma L)^2 \int \frac{P(\Omega-\Omega_1)P(\Omega-\Omega_2)P(\Omega-\Omega_1-\Omega_2)}{(3\tau_{rt}/\tau)\{1+(2\tau L\beta_2/3\tau_{rt})^2\Omega_1^2\Omega_2^2]} d\Omega_1 d\Omega_2$$

and the nonlinear FWM-induced loss term δ_{NL} has the following form:

$$\delta_{NL} = (2\gamma L)^2 \int d\Omega_1 d\Omega_2 \times \tag{N.4.9}$$

$$\times \frac{\left[P(\Omega-\Omega_1)+P(\Omega-\Omega_2)\right]P(\Omega-\Omega_1-\Omega_2) - P(\Omega-\Omega_1)P(\Omega-\Omega_2)}{(3\tau_{rt}/\tau)\{1+(2\tau L\beta_2/3\tau_{rt})^2\Omega_1^2\Omega_2^2]}$$

Here we assumed an exponential decay of the correlation function $\langle E_l(t)E_l^*(t')\rangle = P_l e^{-|t-t'|/\tau}$ with the correlation time τ, and the Gaussian statistics for field $E_m(t)$.

The exponential decay of the correlation function results in the Lorentzian shape of peaks in the Stokes wave inter-mode beating radio-frequency (RF) spectrum:

$$F(\Omega) = \sum_{n \neq 0} \frac{DF_n}{\pi[D^2 + (\Omega - n\Delta)^2]}, \tag{N.4.10}$$

where $F_n = \sum_l P_l P_{l+n}$, and $D = 2/\tau$. So the correlation time $\tau = 2/D$ can be found from the experimentally measured spectral width *D* of the peaks in the RF inter-mode beating spectrum of the Stokes wave.

The last term in the RHS of Eq.(N.4.8) describes an increase of intensity in the mode with frequency Ω due to the scattering of modes with frequencies $\Omega - \Omega_1$ and $\Omega - \Omega_2$ into modes with frequencies Ω and $\Omega - \Omega_1 - \Omega_2$, i.e. this term represents the FWM-induced *nonlinear gain*. The physical meaning of δ_{NL} is the round-trip *nonlinear attenuation* coefficient of the Stokes wave with frequency induced by its scattering on other longitudinal modes with frequencies $\Omega - \Omega_1 - \Omega_2$. It is exactly this nonlinear attenuation that leads to the exponential decay of the correlation function. The nonlinear attenuation increases with power, and completely determines the correlation time at high Stokes power:

$$\frac{\tau_{rt}}{\tau} \simeq \delta_{NL} / 2, \tag{N.4.11}$$

The latter condition makes equations (N.4.7-N.4.9) self-consistent. It is important to stress that the wave kinetic equation (N.4.7-N.4.11) is valid when the average effect of nonlinearity is much less than the average impact of the dispersion:

$$\gamma P \ll \beta_2 \overline{\Omega^2}, \tag{N.4.12}$$

where $\overline{\Omega^2}$ is a mean-square spectral half-width parameter:

$$\overline{\Omega^2} = \frac{\int \Omega^2 P(\Omega) d\Omega}{P}. \tag{N.4.13}$$

Condition (N.4.12) ensures a broad spectral distribution and a phase mismatch between remote spectral components (longitudinal modes). As a result, the FWM-induced phase synchronization is suppressed due to dispersion, and phases of far separated longitudinal modes can be considered as only weakly correlated.

By calculation of the integrals in equations (N.4.8 - N.4.9) in the limit of (N.4.12), one can find the spectral width and the spectral peak power of the Stokes wave assuming that the spectrum is bell-shaped, from the wave kinetic equation For simplicity, but without loss of generality, we consider the case of the cavity reflectors (mirrors) as having Gaussian spectral function. In this case the effective mirror losses have a parabolic form

$$\delta(\Omega) = \delta_0 + \delta_2 \Omega^2. \tag{N.4.14}$$

The integral over the frequency of $S_{FWM}(\Omega)$ is equal to zero, which means that energy is conserved in FWM processes. It follows from Eq. (N.4.7) that

$$\delta_0 + \delta_2 \overline{\Omega^2} = 2gL = 2g_R L \overline{P}_p - 2\alpha L \tag{N.4.15}$$

This equation has a simple physical meaning of equilibrium between the Stokes wave power gain and losses in a single round-trip. In particular, Eq. (N.4.15) links the spectral half-width with the saturated gain g .

Further simplification of the kinetic equation-based analysis can be achieved by replacing frequencies $\Omega_{1,2}^2$ in all denominators of the integrands in the RHS of (N.4.8)-(N.4.9) by corresponding spectrally averaged characteristics. The validity of such replacement should be justified in any specific problem. In particular, this approximation is expected to work well for small spectra. Generally, this approach provides a very illustrative way to describe spectral power dependence. The equations (N.4.9)–(N.4.11) can then be simplified to the wave kinetic equation for the averaged stationary Stokes wave spectrum $P(\Omega)$:

$$[\delta(\Omega) + 2\alpha L + \delta_{NL}]P(\Omega) = \tag{N.4.16}$$

$$= 2g_R L\bar{P}_p P(\Omega) + \frac{\delta_{NL}}{P^2}\int P(\Omega_1)P(\Omega_2)P(\Omega_1+\Omega_2-\Omega)d\Omega_1 d\Omega_2,$$

where δ_{NL} defines nonlinear FWM-induced losses, which can be written in the following form:

$$\delta_{NL} = \sqrt{\frac{2}{3}}\frac{2\gamma PL}{\sqrt{1+(4\beta_2 L\overline{\Omega^2}/3\delta_{NL})^2}}. \tag{N.4.17}$$

Here $P = \int P(\Omega)d\Omega$ is the total intra-cavity Stokes wave power. The round-trip dispersion-induced phase difference between the longitudinal modes is replaced here by the phase difference averaged over the spectrum, $\beta_2\Omega^2 L$, where the mean-square spectral width Ω^2 is defined in (N.4.13).

In the case of a parabolic form of effective losses on cavity mirrors (N.4.14), equation (N.4.16) has a simple analytical solution for the intra-cavity Stokes wave spectrum:

$$P(\Omega) = \frac{2P}{\pi\Gamma\cosh(2\Omega/\Gamma)}, \tag{N.4.18}$$

where the spectral width $\Gamma = 2\sqrt{2\delta_{NL}/(\pi^2\delta_2)}$ and the spectral power density at maximum is $P(0) = 2P/(\pi\Gamma)$. This expression confirms the general prediction that the spectral width Γ increases as the square root of the Stokes wave power P. The maximum of the spectral power density $P(0)$ increases also as a square root of P. Finally, by substituting Eq. (N.4.18) into Eq.(N.4.16) and integrating over Ω, we can describe the dependence of the intra-cavity Stokes wave power P on the pump power $P_p(0)$:

$$\delta_0 + \frac{\delta_{NL}(P)}{2} + 2\alpha L = 2g_R P_p(0)\times\frac{1-\exp(-\alpha_p L - \frac{\lambda}{\lambda_p}g_R LP)}{\alpha_p + \frac{\lambda}{\lambda_p}g_R P}, \tag{N.4.19}$$

where $\delta_{NL} = 2\gamma PL\sqrt{2/3}/[\sqrt{1+(2\beta_2 L/3\delta_2)^2}]$.

N.4.2 Experiments

To experimentally verify the predictions of the theory of weak wave turbulence we studied the spectral broadening of a Stokes wave generated in a one-stage Raman fibre laser (RFL) based on a phosphosilicate fibre [Dianov *et al.*, 1997, 2000] as shown in Fig. N.1. The following parameters characterize the experimental set-up: $\alpha_p = 2.5$ dB/km (including lumped losses, i.e. losses on intra-cavity coupler, excess losses on FBGs, and splice losses), $\alpha = 2.5$ dB/km (including lumped losses), the normal dispersion $\beta_2 \approx 13.3\,\mathrm{nm}^{-2}\mathrm{km}^{-1}$, the nonlinear Kerr coefficient $\gamma \approx 1.5\ \mathrm{km}^{-1}\mathrm{W}^{-1}$, the Raman gain coefficient $g_R = 1.3\,\mathrm{km}^{-1}\mathrm{W}^{-1}$, the length L=370 m. The phosphosilicate fibre has a distinct isolated P_2O_5-related Raman gain peak with a large Stokes shift, which is free from complications induced by overlapping different Raman gain peaks in germanosilicate fibres.

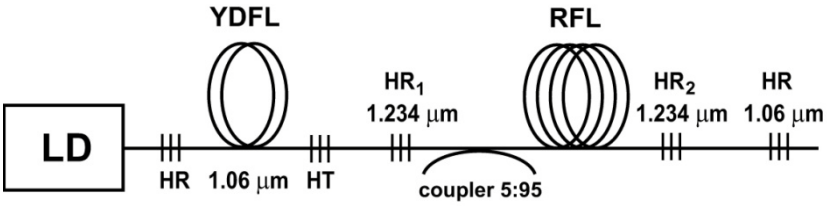

Figure N.1. Schematic diagram of one-stage RFL based on a phosphosilicate fibre.

The pump radiation was produced by a 16 meter long low-Q cavity ytterbium-doped fibre laser (YDFL) operating at the wavelength of 1060 nm. Pump radiation was converted to the first Stokes wave at 1234 nm by the stimulated Raman scattering process in the high-Q RFL cavity of L=370 m formed by P-doped fibre and two fibre Bragg gratings (FBGs) with high reflectivity.

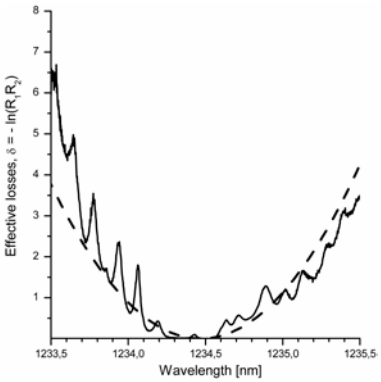

Figure N.2. Effective losses of cavity mirrors used in experiments (solid line) and parabolic approximation (dashed line).

Figure N.2 shows that the spectral profile of losses induced by FBG reflectors $\delta = -\ln(R_1 R_2)$ is indeed well approximated by the parabolic shape. The fitted curvature of the effective FBGs losses is: $\delta_2 = 4\,\mathrm{nm}^{-2}$. Using the intra-cavity coupler, we have measured in details the intra-cavity generated power and spectrum, and compare experimentally measured characteristics with the predictions of the weak wave turbulence theory.

First, let us consider the radio-frequency (RF) spectrum [Babin *et al.*, 2005]. The inter-mode beating peaks in the RF spectrum are diffused, as can be seen from Fig. N.3., the width D of the inter-mode beating peaks increases with power and becomes comparable to the Stokes wave longitudinal modes spacing $\Delta \approx 0.3$ MHz. This observation confirms that there are strong physical mechanisms that de-phase Stokes wave components during a round-trip.

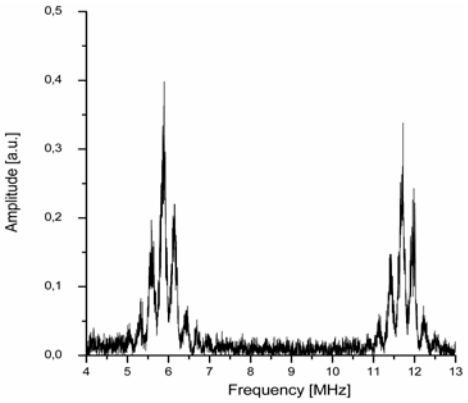

Figure N.3. Experimentally measured RFspectrum of the generated Stokes wave.

Equation (N.4.19) predicts the dependence of the generated power on the pumping power. Figure N.4 shows remarkable agreement between the theoretically calculated and measured intra-cavity Stokes wave power P.

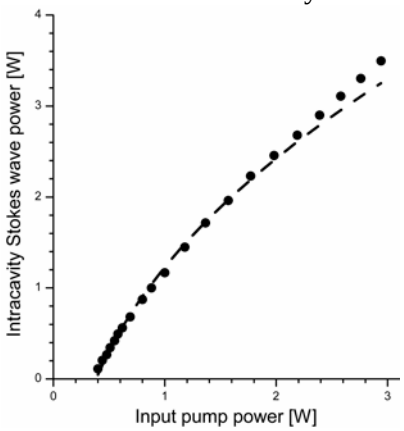

Figure N.4. Experimentally measured (dots) and theoretically calculated (dashed line) total intra-cavity Stokes wave power generated inside the Raman fibre laser.

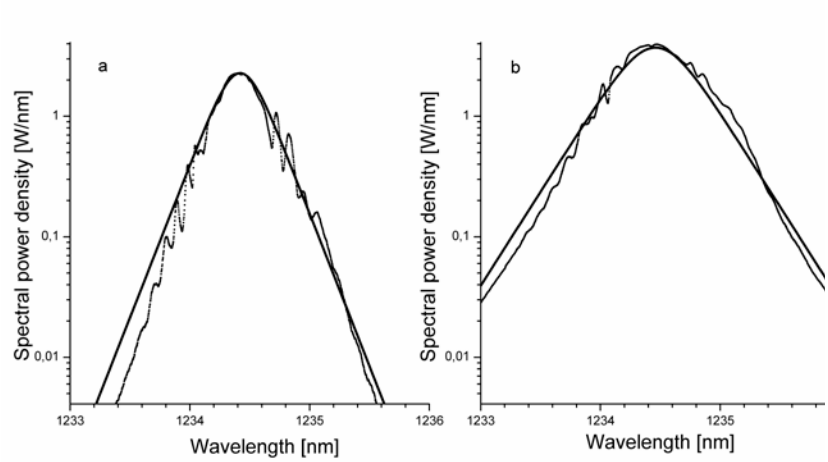

Figure N.5. Experimentally measured (dots) and theoretically calculated (solid line) total intra-cavity Stokes wave generation spectra at different pump power: (a) 2W; (b) 3 W.

Using Eq. (N.4.18) one can easily calculate the Stokes wave spectral profiles $P(\Omega)$ at different intra-cavity Stokes wave power levels P. Figure N.5 shows an excellent agreement between experimentally measured and theoretically calculated spectra in a broad power range.

We would like to stress that *no fitting parameters were used* in the comparison shown in Fig. N.5. It is quite remarkable that a theory based on quite a few assumptions gives such a good analytical description for the observed RFL generation spectra. A specific feature of the spectra is their exponential tails. The oscillations in the experimentally measured profiles correspond to the ripples in the FBG losses profile. Note that the measured Stokes wave spectra are averaged over the standard resolution ~ 0.01 nm of a spectrum analyzer, that corresponds to $\sim 10^4$ longitudinal modes, while their total number is $\sim 10^6$. That justifies the averaging over $\sim 10^4$ longitudinal modes that was used in the derivation of the wave kinetic equation for the Stokes wave.

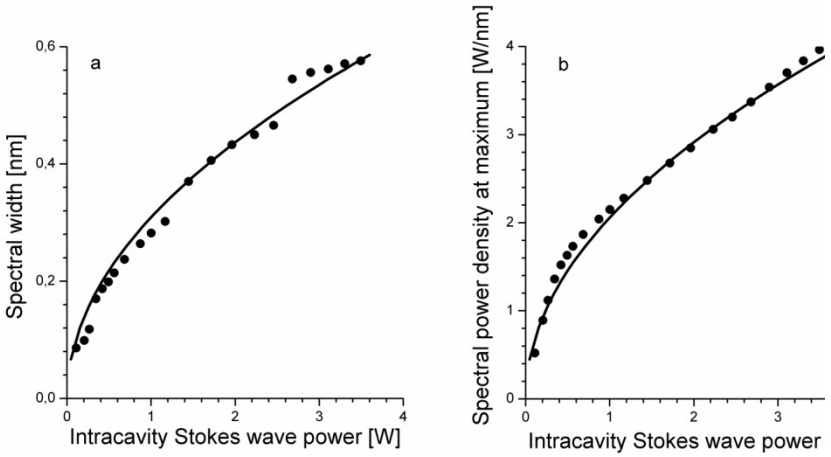

Figure N.6 .Experimentally measured (dots) and theoretically calculated (solid line) spectral width (a) and spectral power density at maximum (b).

Figure N.6 confirms the specific prediction of the wave turbulence theory: square-root dependence given by Eq. (N.4.17) and (N.4.18) for the Stokes wave spectrum broadening with the growing generated power. The comparison between the experimental data and results of numerical calculation is shown both for the spectral width and a maximum of the spectral power density. Again a very good agreement between theory and experiment is demonstrated.

It is also important that one of the key RFL characteristic - the output RFL power $P_{0,L}^{out}(\Omega) = -\ln R_{0,L})P^{\mp}(\Omega)$ - can also be easily found applying the theory developed in previous Sections. In the case of identical Gaussian cavity mirrors the running Stokes wave power is $P^{\pm}(\Omega) \simeq P(\Omega)/2$ which results in

$$P_{0,L}^{out}(\Omega) = \frac{\delta_0 + \delta_2 \Omega^2}{2} \frac{I}{\pi \Gamma \cosh(2\Omega/\Gamma)}. \qquad \text{(N.4.20)}$$

A more detailed analysis of the output power in the case of highly transmitting output FBG is performed in [Babin et al, 2008a].

N.4.3 Statistical properties and optical rogue wave generation via wave turbulence in Raman fibre lasers

Extreme value statistics in nonlinear fibre optics have attracted great attention since the experimental demonstration of optical rogue waves in supercontinuum (SC) [Solli *et al.*, 2007]. The statistics of extreme events have already been studied in a number of optical systems including pulsed and CW pumped SC sources [Dudley *et al.*, 2008], silicon [Bourlaug *et al.*, 2009] and fibre [Hammani *et al.*, 2008] Raman amplifiers, optical filamentation [Kasparian *et al.*, 2009], optical data transmission [Vergeles and Turitsyn, 2011] and others.

There is a variety of nonlinear optical systems with rather different physical mechanisms attributed to the emergence of the rare intense events. In the case of SC generation, the extreme events are defined by the complex interplay of the modulation instability, third-order dispersion and collisions of Raman-shifted solitons [Dudley *et al.*, 2008; Mussot *et al.*, 2009]. The analysis of coherent nonlinear structures e.g. the breathing solutions of the nonlinear Schrödinger equation provides useful insight into the physics of rogue waves in optical system [Akhmediev *et al.*, 2009; Akhmediev, Soto-Crespo *et al.*, 2009; Dudley *et al.*, 2009] and classical problems of rogue waves appearance on the water surface [Kuznetsov 1997; Kawata and Inoue 1978; Akhmediev and Korneev 1986; Peregrine 1984; Shrira and Georgajev 2007; Kharif *et al.* 2009; Zakharov and Gelash 2011; Dyachenko and Zakharov 2011; Chabchoub *et al.*, 2011].

The rare occurrence of large amplitude waves, certainly, is not restricted to systems with coherent structures. In Raman amplifiers [Hammani *et al.*, 2008] and Raman parametric amplifiers [Hammani *et al.*, 2009], the main mechanism is the exponential transfer of the intensity fluctuations from the pump wave to the signal via a Raman response, which can be significantly enhanced in the case of the weak walk-off parameter [Hammani *et al.*, 2008]. Similarly, in the optical filamentation processes the noise transfer from the pump plays a key role [Kasparian *et al.*, 2009]. It has been also observed that sporadic rogue wave events emerge from turbulent fluctuations and manifest themselves as bursts of light during the propagation of the optical wave along the long fibre [Hammani *et al.*, 2010].

It is likely that extreme rare events could also occur in the partially coherent (PC) continuous-wave (CW) fibre lasers as the radiation of such systems presents a large number of longitudinal modes. Here we examine the emergence of intense rare events through optical wave turbulence in the high-Q cavity RFL. The spectral, temporal and statistical properties of the Raman fibre lasers can be calculated numerically from the system of coupled NLS equations [Agrawal, 1995]:

$$\pm\frac{\partial A_p^{\pm}}{\partial z}+\beta_{1p}\frac{\partial A_p^{\pm}}{\partial t}+\frac{i}{2}\beta_{2p}\frac{\partial^2 A_p^{\pm}}{\partial t^2}+\frac{\alpha_p}{2}A_p^{\pm}=$$

$$=i\gamma_p\left(\left|A_p^{\pm}\right|^2+2\left|A_s^{\pm}\right|^2\right)A_p^{\pm}-\frac{g_p}{2}\left(\left|A_s^{\pm}\right|^2+\left\langle\left|A_s^{\mp}\right|^2\right\rangle\right)A_p^{\pm} \qquad \text{(N.4.21)}$$

$$\pm\frac{\partial A_s^{\pm}}{\partial z}+\beta_{1s}\frac{\partial A_s^{\pm}}{\partial t}+\frac{i}{2}\beta_{2s}\frac{\partial^2 A_s^{\pm}}{\partial t^2}+\frac{\alpha_s}{2}A_s^{\pm}=$$

$$=i\gamma_s\left(\left|A_s^{\pm}\right|^2+2\left|A_p^{\pm}\right|^2\right)A_s^{\pm}+\frac{g_s}{2}\left(\left|A_p^{\pm}\right|^2+\left\langle\left|A_p^{\mp}\right|^2\right\rangle\right)A_s^{\pm}$$

where A is the complex field envelope, z is a coordinate, t stands for time, $v_s=1/\beta_{1s}$ and $v_p=1/\beta_{1p}$ are Stokes and pump waves group-velocities, respectively, β_2, α, γ,g are dispersion, linear attenuation, Kerr and Raman coefficients, $\pm$ denote counter-propagating waves, "s" and "p" are used for Stokes and pump waves. Angular brackets here denote averaging over time that is applied to reflect the fact of very large walk-off (difference in group velocities) between waves moving in opposite directions effectively leading to averaging of the impact from the counter-propagating waves. Alternatively, one can use the exponential approximation for the pump wave instead of a separate equation for pumping waves (see e.g. [Randoux *et al.*, 2011; Falkovsky 2004] for details).

Currently, it is not practical to solve the Cauchy problem numerically to model the radiation generation in a typical fibre laser due to a level of required computational resources. Therefore, in (N.4.21) the powers of counter-propagating waves are included through their average effect. This is justified by the observation that counter-propagating waves move

fast with regard to each other and, as a result, the overall impact is averaged out as in (N4.21). Equations (N.4.21) are integrated along z using the iterative approach, i.e. when integrating equations for $A^{+}_{s,p}$ we used $A^{-}_{s,p}$ obtained on the previous iteration, and vice versa. Note that, strictly speaking, model (N.4.21) is not a system of equations in the mathematical sense, i.e. we don't solve these equations simultaneously. We solve the equations for forward and backward propagating waves one by one, i.e. forward propagating wave on the n-th roundtrip interacts with backward propagating wave on the (n-1)-th roundtrip which is already computed. The boundary conditions at the edges of resonator are standard reflection conditions imposed by the FBGs or other reflectors. Similar iterative procedures have been used in the numerical modeling of RFL [Randoux *et al.*, 2011], Ytterbium doped-fibre lasers [Turitsyn *et al.*, 2011], Brillouin fibre lasers [Preda *et al.*, 2011]. Note that in this laser system the exponential transfer of fluctuations from the pump wave to the generation wave (XPM between pump and Stokes waves) does not make any significant contribution to dynamics well above the generation threshold (see Fig. N.7). Effectively, the corresponding terms proportional to $\gamma A_s A_p^2$ could be omitted in the equations (N.4.21).

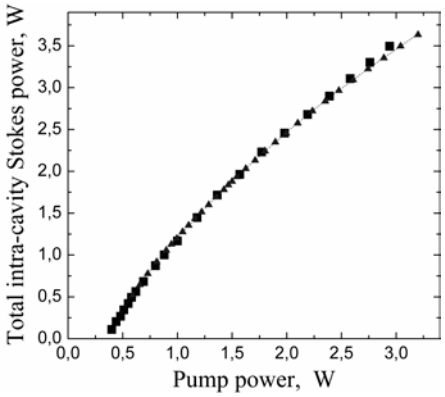

Figure N.7. Total generated intra-cavity power: experimental (squares), numerically calculated without XPM (dotted line) and with XPM (triangles)

Computations show that the generation becomes stable after about 10^2-10^4 round-trips depending on the power. Results do not depend on grid size at 2^{12}-2^{16} grid points. We checked that, neither decreasing the

time steps, nor increasing the numerical window, affect the results. The following coefficients have been used in numerical modeling: α_p = 0.5 $(km)^{-1}$, α_s= 0.83 $(km)^{-1}$, (α values also include lumped losses on splices, couplers and so on), β_{2p} = 17.9 ps^2/km, β_{2s}=7.17 ps^2/km, γ_s= 3 $(km*W)^{-1}$, g_s=1.3 $(km*W)^{-1}$, the cavity length L=370 m.The computed generated total intra-cavity Stokes wave power agrees rather well with the experimental data (Fig. N.7) and analytical theory (compare with Fig. N.4).

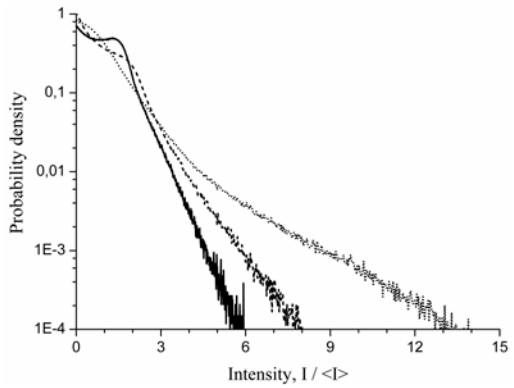

Figure N.8. Intensity PDF of the total intra-cavity (black line), reflected back to the cavity from the laser mirror (dashed line) and output (dotted line) laser radiation.

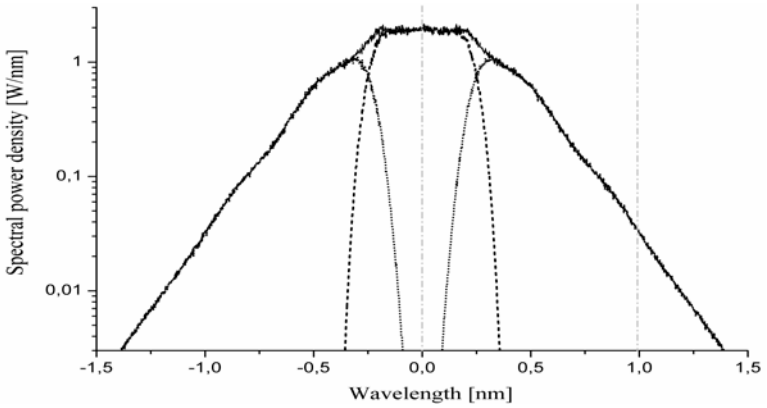

Figure N.9. Total intra-cavity (black line), reflected from the laser mirror (dashed line) and output (dotted line) spectrum generated in high-Q cavity RFL. Vertical dashed lines indicate the central positions of two spectral.

Properties of radiation can be manipulated by using different spectral shapes of reflectors (see e.g. [Turitsyna, *et al*., 2010] and also Section N.5.3). Considering the super-Gaussian FBGs of 0.5 nm width we have found that the statistical properties of generated radiation are different for the intra-cavity radiation incident on the laser mirror, radiation reflected back to the cavity by the mirror and the output radiation as shown in Fig. N.8. Randoux *et al* [Randoux *et al.*, 2011] observed that the amplitude PDF changes its shape during propagation from one laser mirror to another

The origin of the difference in statistical properties before and after transmission/reflection at the laser mirror can be understood as follows. The generation spectrum well above the threshold is broader than the spectral profiles of the laser mirrors, as seen in Fig. N.9.There are two principally different parts in the spectrum: the central part and the spectral wings. As the laser mirrors are highly reflective, the central part of the spectrum is built during many cavity trips. Turbulent-like four-wave mixing processes [Babin *et al.*, 2007a] lead to the generation of the spectral wings. Being detuned from the spectrum centre by more than laser reflector (mirror) bandwidth, the far spectral wings are out-coupled from the cavity at every round trip at each mirror. Therefore, effectively they are generated at single pass only. Thus, the statistical properties of the intra-cavity radiation, in general are defined mainly by the central part, rather than by the spectral wings. The power in the central part is several times higher than the power in the wings. On the contrary, the statistical properties of the out-going radiation are defined mainly by the spectral wings, as the central part is filtered out by the laser mirrors.

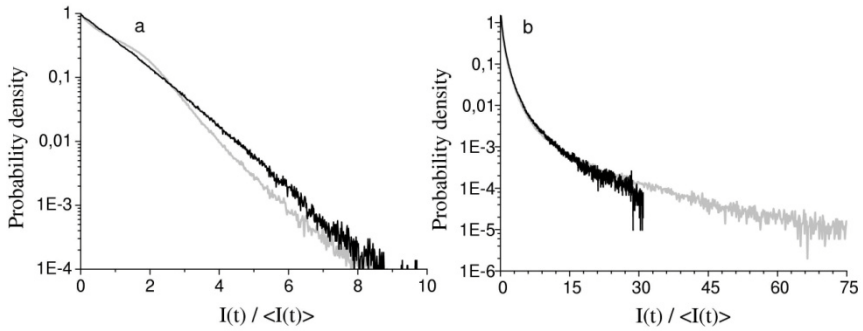

Figure N.10. Intensity PDF of the modes filtered out from the (a) spectrum center and (b) spectral wing (filter is detuned by 1 nm from the spectrum center). Filters spectral full widths are 0.1 nm (black) and 0.5 nm (gray)..

Since the intensity (power) PDF of the intra-cavity radiation is sufficiently non-exponential, it means some correlations between different longitudinal modes do exist [Churkin *et al.*, 2010]. Using spectral filters of different spectral widths centered at different spectral positions (filter 1 is centered at the maximum of generated spectrum, filter 2 is detuned by 1 nm from the spectrum center), we can calculate the intensity PDF of a specific part of the generation spectrum. It is found that the intensity PDF of the modes generated on the flat top at the spectrum center is exponential (Fig. N.10a). With the increase of the filter bandwidth, the PDF deviates more and more from the exponential. The statistics of the central part of the spectrum is close to the Gaussian one. However, the statistics of the distant spectral components are more influenced by nonlinear phenomena in the Raman fibre laser. Deviations from the exponential form of the intensity PDF of spectral components at far spectral wings reveal the occurrence of rare events – waves with high amplitude occur with a probability higher than that given by the corresponding Gaussian distribution (Fig. N.10b). The extreme value events are more pronounced in the output radiation of the high-Q cavity RFL. It is interesting to note that the self-filtering of extreme events by the laser mirror is similar to the designed spectral filtering approach used previously in Raman fibre amplifiers [Finot *et al*., 2009].

Extreme value events can be detected from the analysis of the time series of generated radiation. The temporal behavior of the total intra-cavity radiation is irregular with the occurrence of high amplitude

fluctuations having an amplitude several times higher than the mean value as seen in Fig. N.11a. This kind of temporal intensity evolution is typical for stochastic signals, which consist of many independent modes with the Gaussian statistics. However, the situation is dramatically changed considering the output radiation that produces the rare fluctuations has amplitude more than 100 times higher than the average output power in the given spectral region (Fig. N.11b).

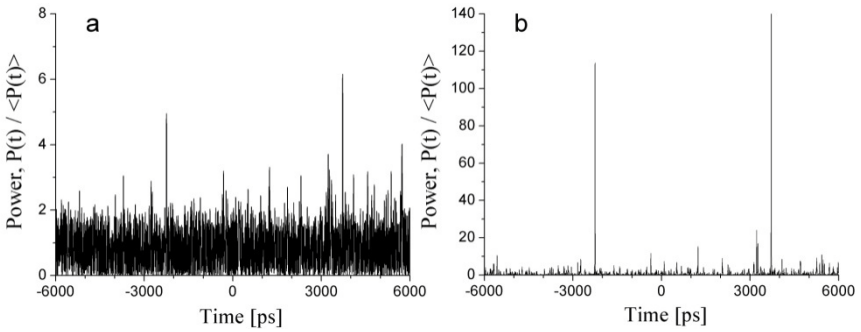

Figure N.11. (a) The time dynamics of the total intra-cavity radiation and (b) radiation generated within the 0.5 nm spectral width at the far spectral wing..

The typical temporal width of such extreme rare event at the laser output is about 5-10 ps. This makes it difficult to detect them directly in real-time, as such events occur irregularly.

Rogue waves of high amplitude are generated in RFLs at far spectral wings, thus such waves are generated in a one cavity pass only. However, the physical mechanism of rare events in RFLs is different from those observed in Raman fibre amplifiers. In RFAs the signal propagating along the fibre acquires the intensity fluctuations from the pump wave which can evolve into extreme amplitude pulses under conditions of self-induced modulation instability [Hammani *et al.*, 2008]. In Raman fibre lasers, the noise transfer from pump wave to the generation wave is negligible. The key role is played by the effect of turbulent four-wave mixing of a multitude of longitudinal modes in the generated Stokes waves [Babin *et al.*, 2007a]. Occurrence of rogue waves is statistical, resulting from turbulent interactions leading to the generation of far spectral components of very high amplitude. The turbulent mechanism of

extreme waves generation in RFLs can be potentially described using the formalism of wave turbulence similar to of propagating waves in a long fibre by [Hammani *et al.,* 2010]. The similar mechanism of extreme wave generation can be important in other types of fibre lasers including lasers operating via random distributed feedback [Turitsyn *et al.,* 2010; Fotiadi *et al.*, 2011].

N.5. Optical wave turbulence in ultra-long fibre lasers

The number of generated modes increases with the lengthening of the fiber cavity that may influence their turbulent interaction and laser characteristics, as a result. Although the concept of ultra-long Raman fibre laser (URFL) architecture was initially proposed and implemented for development of a quasi-lossless signal transmission scheme, see e.g. [Ania-Castañón *et al.,* 2006] and references therein, the problem is more general: a substantial increase of the RFL cavity length leads to a new interesting class of lasers with potentially different physical mechanisms underlying their operation. In this context, various fundamental questions arise: What are the limits of the cavity length for laser operation? What are particular spectral features of ultra-long RFLs – cavity mode structure, output spectrum and corresponding temporal properties of the radiation generated inside the cavity?

We address these questions through the analysis of the spectral and temporal characteristics of ultra-long RFLs with cavity lengths from 6.6 km to 84 km operating at 1455 nm, and up to 270 km for 1550-nm laser operating just in the fibre transparency maximum. We will show that important characteristics of such ultra-long fibre lasers can be directly explained by the occurrence of weak turbulent-like interactions of a huge number (~100 millions in URFL) of longitudinal laser modes.

N.5.1 Basics of ultra-long fibre lasers{ XE "parts" }

The basic design of the ultra-long laser cavity studied in this work is schematically depicted in Figure N.12. Without a loss of generality, as a first step, we consider an URFL designed to provide distributed signal amplification in the telecommunication window at 1550 nm similar to the

scheme treated in [Ania-Castañón *et al.*, 2006]. However, we would like to stress that the concept of URFL presented here is very general and is not limited to wavelengths considered in this paragraph.

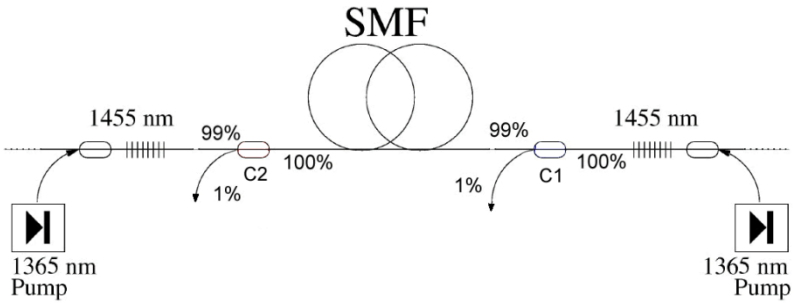

Figure N.12. Schematic depiction of the ultra-long Raman fibre laser.

The URFL system (see Figure N.12) consists of two equal-power depolarized primary Raman pumps with a nm-broad spectrum centered at 1365 nm which are launched from both ends of the standard single-mode fibre (SMF) span. Two highly reflective FBGs (reflection coefficient is 98% at 1455 nm) were used at each end of the fibre span. This results in the formation of a high-Q cavity trapping the first Stokes counter-propagating waves between the two FBGs. When the power of the primary pumps is above the required threshold for the Raman gain to overcome the fibre attenuation, the laser starts to generate radiation at the Stokes wavelength of 1455 nm. Two 99:1 couplers were placed near the FBGs at the right (C1) and left (C2) ends of the span to monitor the generated intra-cavity Stokes wave power P and its optical and radio frequency (RF) spectra.

The RF spectrum, monitored using a photodetector and an electrical spectrum analyzer, displays inter-mode beating peaks with a clear mode structure despite the large cavity length up to some critical power. The optical spectrum of the generated Stokes wave was monitored through an optical spectrum analyzer with a resolution of ~0.01 nm. The Stokes wave power was measured by a power meter, whereas its temporal behaviour was studied with a fast oscilloscope with a 50 ps resolution.

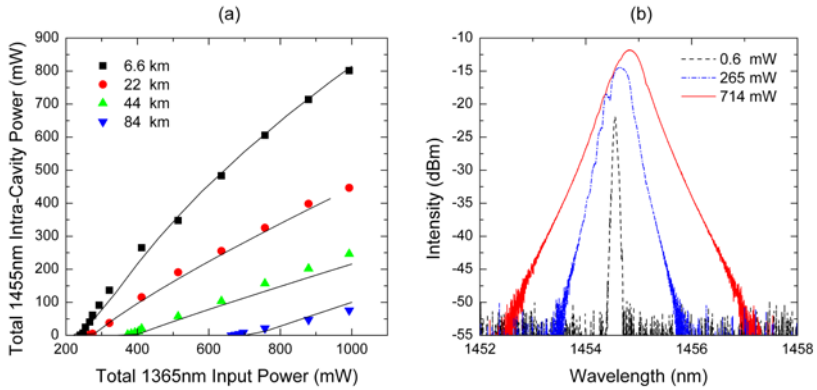

Fig. N.13: (a) Total intra-cavity power at 1455 nm as a function of the total pump power at 1365 nm: experimental points and numerical simulation (solid curves) . (b) 1455 nm spectrum measured at point C2, Stokes power =0.6, 265 and 714 mW for L=6.6 km.

Figure N.13(a) shows the total intra-cavity power P of the Stokes wave (1455 nm); measured via the 1% port at point C2, as a function of the total pump power at 1365 nm. The generated power exhibits typical laser behaviour. Above the threshold required for the SRS to overcome fibre attenuation ($\alpha_{1455}\approx 0.25$ dB/km) and lumped losses of FBGs, couplers and connections ($\delta_0 \approx 1.4$ dB), the laser starts generation at 1455 nm. Experimental results are in good agreement with modelling (solid lines in Fig. N.13(a)) of the cavity modes dynamics using ordinary differential equations similar to Eq. (N.4.21) describing four-wave mixing interactions [Babin *et al.*, 2008b].

Though the governing dynamical equations are deterministic, the solutions should be treated as a result of an irregular process: the FWM nonlinear process engages a huge number of rapidly oscillating terms with different amplitudes and phases. Above the threshold, the Stokes wave power grows nearly linearly with increasing pump power. As expected, the longer the cavity, the lower the generated 1455 nm power, due to higher cavity losses caused by the attenuation of the pump ($\alpha_{1365}\approx 0.31$ dB/km) and Stokes waves, which raise the threshold. The measured experimental threshold for URFL [Babin *et al.*, 2008b] are in complete agreement with the simple theoretical RFL model, which was confirmed earlier by experiments with short fibre spans [Babin et al., 2003]. For longer spans, distributed losses remain the main factor and the

threshold is nearly proportional to the length. Despite this, even for the longest cavity length of 84km, the threshold pump power is rather small, ~0.7 W.

The evolution of the intra-cavity Stokes wave optical spectra is shown in Fig.N.13(b) for the 6.6 km case. The spectrum is rather narrow near the threshold and broadens with increasing pump power. Furthermore, the broadened spectrum acquires clear exponential tails for all cavity lengths studied, similar to a conventional RFL, see Fig. N.5.To trace how the spectral structure is affected by the boundary condition, we used FBGs with ripples in the short-wave wing of their reflection profile. Figure N.13(b) shows that the spectrum for Stokes power = 265 mW has the same low wavelength ripples as the FBGs, which are not seen for Stokes power = 714 mW: the generated spectra follow the FBGs reflection profile at low powers, but are not influenced by the boundary conditions at higher powers. A drift towards longer wavelengths with increasing power was observed, but measurements of the gratings spectral response revealed a shift of the central wavelength of the FBGs - attributed to thermal expansion- as the cause.

The broadening mechanism and its dependence on input power can be understood from the analysis of the interaction between the intra-cavity longitudinal modes based on the weak wave turbulence model of the RFL [Babin et al., 2007a]. The turbulent-like interaction of the modes also results in stochastic behaviour of the integral power in the time domain exhibiting fluctuations in various time scales with an amplitude of noisy spikes reaching levels exceeding the average level by over 50%.

N.5.2 Mode structure in ultra-long fibre lasers

The existence of a longitudinal mode structure is one of the most important laser characteristics. It has been shown [Babin et al, 2005] that for a Raman laser with L=0.37 km cavity length, a corresponding Raman fibre laser (RFL) mode structure with spacing as small as $\Delta = c/2nL \sim 0.3$ MHz (n is refractive index, c is the speed of light in vacuum) is observable in its RF spectrum, see paragraph N.4.2. At the same time, the observed peaks are broadened significantly with the increasing power of

the intra-cavity generated Stokes wave indicating the impact of the nonlinear interactions of modes. An increase of the cavity length should proportionally reduce the mode spacing, which may be critical for resolving the mode structure. In this paragraph we review the measurement techniques and the results of mode structure analysis in ultra-long Raman fibre lasers with cavity length varying from L=6.6 km to L=84 km presented in [Babin *et al*., 2007b].To examine the mode structure of the URFL cavity, the signals from the 1% splitter ends (see Fig.N.12) were analyzed using the fast photodiode and electrical spectrum analyzer with a resolution of <400Hz, to obtain RF spectra in which inter-mode beating can be observed as being similar to conventional RFL [Babin *et al*., 2005].

The results of the RF beating spectra, measured slightly above the generation threshold, are presented in Fig. N.14. It is clear that the inter-mode beating peaks are resolvable for all cavity lengths studied, and that the spectral spacing Δ between them follows the classical formula $\Delta=c/2nL$. For the cavity length L=84 km, the corresponding mode spacing is as low as $\Delta\approx1.2$ kHz, while the width of the RF peaks is narrowed to hundreds of Hz. Furthermore, we have observed the broadening of the modal peaks for all the considered cavity lengths as the intra-cavity power is increased (see Fig. N.15). Figure N.16 shows the measured spectral width (full width at half a maximum, i.e. spectral width at -3 dB level) of the RF peaks versus the total intra-cavity power. Here several points (105 to 270 km cavity) have been added from the measurements of a different laser configuration that will be discussed in detail in Section N.5.5. It is clearly seen that the spectral width of the RF peaks depends on the intra-cavity power in a nearly linear manner, and is almost independent of the fibre span length [Turitsyn *et al.*, 2009].

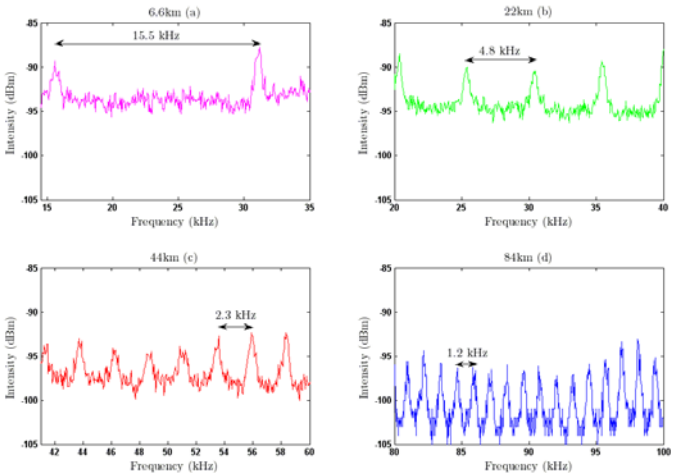

Figure N.14 Ultra-long RFL RF spectra measured via the 1st splitter for different cavity lengths 6.6 km (a), 22 km (b), 44 km (c), 84 km (d) at total intra-cavity power P≈7 mW at 1455 nm.

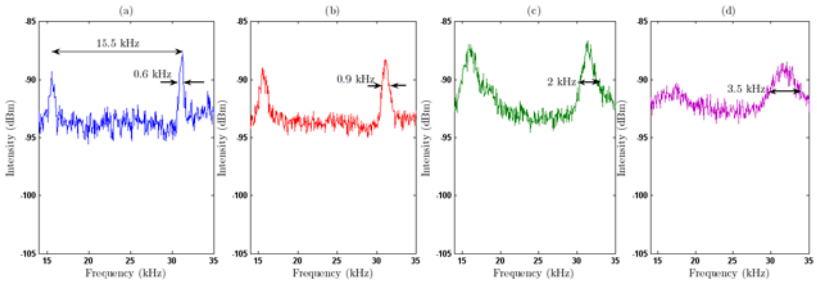

Figure N.15. RF spectra measured via the 1st splitter for the RFL with cavity length L=6.6 km at different total intra-cavity power at 1455 nm (a) P≈7 mW, (b) 61 mW, (c) 136 mW, (d) 265 mW.

The width values extrapolated to zero power nearly corresponds to the nameplate resolution of the electric spectrum analyzer used. One quite intriguing observation from the presented results is that propagation in such a long span does not drastically impact the relative phases of the modes, resulting in narrow RF peaks at low powers. This illustrates standing wave formation between the reflectors of the linear Fabry-Perot cavity with a length of ~100 km. The result is contrary to a natural

expectation that various effects such as thermal noise and fibre span fluctuations would lead to mode de-phasing in such long laser cavities.

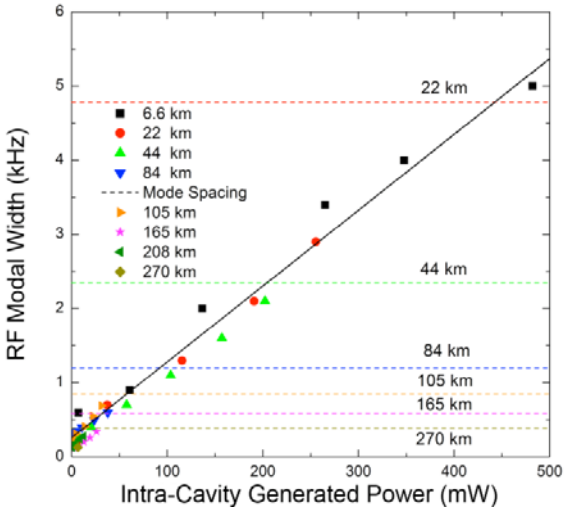

Figure N.16. Mode beating peak width (FWHM) for 6.6, 22, 44, 84, 105, 165, 208 and 270 km lasers (differently marked points) and their linear fit. Corresponding mode spacing values are shown by horizontal lines.

It was expected that with the growing intra-cavity power nonlinear optical effects play an increasingly important role in determining laser characteristics. The role of nonlinear effects in the RF spectra of relatively short RFL with high-Q cavity has been treated in [Babin *et al.*, 2007a] in the framework of the weak turbulence theory, see paragraph N.4.1. It has been suggested that with increasing intensity of laser radiation, the main contribution to de-phasing of Stokes waves in the cavity comes from the effective "nonlinear attenuation" effect arising from the FWM-induced turbulent-like interaction of waves with different frequencies (corresponding to different cavity modes). This de-phasing process is greatly enhanced in the ultra-long cavity because of the significantly larger number of interacting modes. In the case of URFL the mode number estimated as the ratio of the optical spectrum width and the mode spacing is really huge (10^7-10^8), which enhances stochastic effects.

We would like to stress that such a stochastic, turbulent-like behaviour of the modes leads to a rather specific broadening of the RF

spectra, proportional to the intensity generated. The width of the inter-mode beating peaks *D* appears almost independent of the cavity length and grows linearly with increasing Stokes wave intensity *P* confirming the major role of nonlinear attenuation and the stochastic nature of the cavity mode interactions, see Eq. (N.4.10), (N.4.11).

At the same time, the mode spacing $\Delta=c/2Ln$ decreases with cavity length from $\Delta\sim15.5$ kHz at L=6.6 km to $\Delta\sim1.2$ kHz at L=84 km. The power limit for a resolvable mode structure may be defined as the value for which the modal width equals the mode spacing (i.e. $D \approx \Delta$). Higher powers result in the generation of "modeless" stochastic spectra with an exponential-wing envelope.

It has been demonstrated in [Turitsyn *et al.*, 2009] that the mode structure of the ultra-long fibre laser can be resolved up to a record cavity length of 270 km. As we will show below, with further increase of of the laser cavity, the Rayleigh scattering starts to play a critical role in limiting resolvable mode operations of URFL. The very narrow RF peaks reveal that the relative phase fluctuations between the neighbouring modes remains very small (at low power), even propagating through such a long span. These results prove the feasibility of a new class of laser with ultra-long cavity. At the same time, significant turbulent de-phasing occurs with an increase of the generated RFL power to the level of tens of mW inside the ultra-long cavity due to their interaction via multiple four-wave mixing nonlinear processes. As such, the model of optical spectra formation in URFLs based on the treatment of modes with random phases may be developed, which is done in the next paragraph.

N.5.3 Nonlinear broadening { XE "chapters" }of optical spectra

Typical intra-cavity spectra generated by the URFL were shown in Fig.N.13(b). Extending the laser cavity to L>100 km greatly increases the number of modes ($\sim10^8$), enhancing the effects of wave turbulence. This is confirmed by the strong broadening of the Stokes spectrum, which is significant even at *mW* level (see Fig. N.17.). The spectrum has well-defined exponential tails. The spectral width of the Stokes wave increases nonlinearly with power, as seen in Fig.N.17, and does not vary

significantly with length for identical powers. A square-root fit appears to be a good approximation of the spectral width dependence on the power at -3 dB level, as predicted analytically [Babin *et al.*, 2007]. Note, however, that the analytical theory is not directly applicable in the case of ultra-long Raman fibre lasers.

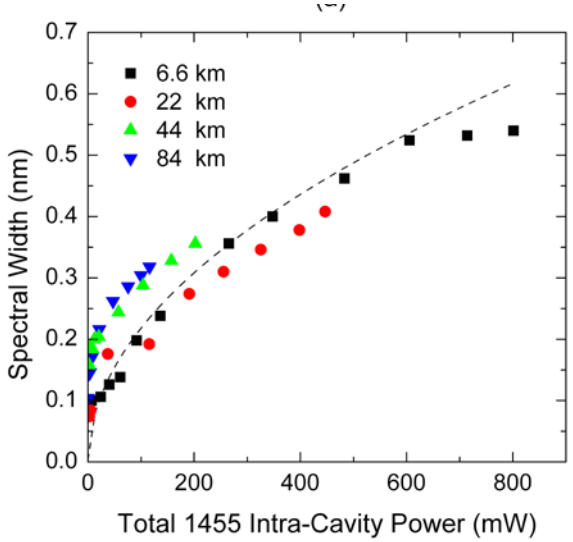

Figure N.17 Spectral widths at -3 dB of power distribution at 1455 nm as a function of the total 1455 nm power for different fibre cavity lengths L=6.6; 22; 42 and 84 km. The dashed lines represent the fit by function $y=Ax^{1/2}$.

The analysis of the impact of the FBG reflection profile demonstrates the washing out of the FBG-induced ripples after propagation through the fibre at high powers. Using an additional splitter at intermediate points, we observed that the spectrum acquired its characteristic exponential tails without ripples after <6 km and propagates further in the cavity without broadening. Therefore, we conclude that system memory of the FBG profile is lost in the nonlinear turbulent evolution of cavity modes. Experimental results are in good agreement with the modelling of modes dynamics using ordinary differential equations describing four-wave mixing (FWM) interactions [Babin *et al.*, 2008b]. It was also shown later by detailed numerical analysis [Soh *et al.*, 2010] that the nonlinear broadening (after kilometers of propagation) is stabilized by dispersion.

The new class of ultra-long lasers is characterized by a range of particular properties, such as the exponential wings of the generated optical spectra, which broaden nonlinearly (close to square-root) with increasing intensity. Their mode structure is resolvable in the RF spectra, in a limited power interval from the generation threshold up to a maximum power dependent on cavity length. Above a given power value, the stochastic mode de-phasing due to uncorrelated fluctuations of mode frequencies induced by FWM leads to broadening prevailing over mode separation and to the generation of a "modeless" or "quasi-continuous" spectrum. In extremely long cavities (>270 km) spectrum is modeless even at the lasing threshold, because of the distributed feedback provided by the Rayleigh backscattering, see [Turitsyn et al., 2009].

N.6 Developed optical wave turbulence in fibre lasers

N.6.1 The impact of fibre dispersion

In treating a large number of interacting modes (up to 10^8 for long cavity fibre lasers) sharing between them a finite generated power, one can assume the phases of different modes to be random and the interaction to be weak (weak-turbulence approach described in [Zakharov *et al.*, 1992]). In quantitative terms, this can be expressed as the following condition on the effective nonlinearity/dispersion ratio

$$\xi = \gamma P / |\beta_2| \Omega_{rms}^2 << 1 \qquad \text{(N.6.1)}$$

Here $P = \sum_m |E_m|^2$ is total generated power,

$$\Omega_{rms} = \sum_m m^2 |E_m|^2 / \sum_m |E_m|^2 * \Delta$$

is spectral bandwidth, Δ –spectral separation between modes. In the weak wave turbulence approach the results would be *insensitive to the sign of wave dispersion* β_2. However, it was demonstrated [Turitsyna *et al.*, 2009] that the change of the dispersion sign dramatically affects the spectral shape and statistics of the laser radiation. The observed wave

turbulence cannot be treated in terms of weak wave turbulence as the impact of nonlinear interactions is not small compared to other effects. Properties of the turbulent behaviour of generated radiation present an example of the developed wave turbulence with strong nonlinear interactions between waves.

The main difference between the cases of normal ($\beta_2>0$) and anomalous ($\beta_2<0$) dispersion is a modulation instability, which exists at $\beta_2<0$. For normal dispersion, the CW is stable with respect to infinitesimal perturbations. As we will show the effect of dispersion on wave turbulence is rather nontrivial. The stable CW can be formed in the case of normal dispersion $\beta_2>0$, however, nonlinear interaction between several modes corresponding to real world CW can lead to rather complicated dynamics leading effectively to a nonlinear instability of CW. Overall, this might add to a further spectrum broadening due to four-wave mixing. Spectrum broadening at $\beta_2>0$ is due to the competition between FWM and dispersion, so that one can expect that the width is determined by the balance of dispersion and nonlinearity, $|\beta_2|\overline{\Omega}_{rms}^2 \cong \gamma P$, i.e. comparable to that determined by modulation instability (MI).

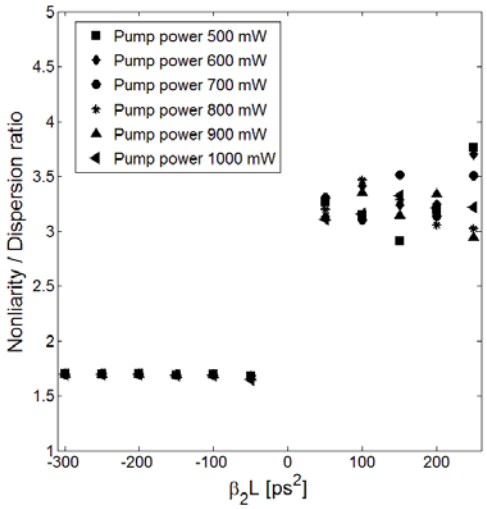

Figure N.18 Nonlinearity / Dispersion ratio for different values of β_2.

This is confirmed by direct numerical modeling of Eq. (N.3.6). Indeed, as seen in Fig. N.18, ξ practically does not depend on $|\beta_2|L$ and the pump power. In the interval of pump powers between 500 mW and 100 mW: ξ =1.7 for $\beta_2<0$ and ξ = 3.3 for $\beta_2>0$. It is seen that the spectral width is such that the effective dispersion is almost twice larger for $\beta_2>0$ when it must balance nonlinearities, MI and four-wave mixing, acting together to widen the spectrum. Since $\xi>1$, the system behaviour cannot be explained by the weak-turbulence approximation in all these cases.

Figure N.19 shows the average spectra of generated radiation after many round trips. While the integral characteristics such as the root-mean- square spectral width are comparable, the spectra for anomalous dispersion, $\beta_2<0$, are smoother and have a characteristic triangular shape with more narrow peaks compared to more concave and irregular spectra for normal dispersion, $\beta_2>0$. In the experiment we have studied two Raman fibre lasers with the cavities of 13.5 km built of two commercially available fibers - SMF (single mode fibre), with anomalous dispersion β_2=-11.63ps^2/km (here $\beta_2 L$ ~ -157 ps^2) and IDF (inverse dispersion fibre) with normal dispersion β_2=36.44 ps^2/km (here $\beta_2 L$~ 492ps^2).

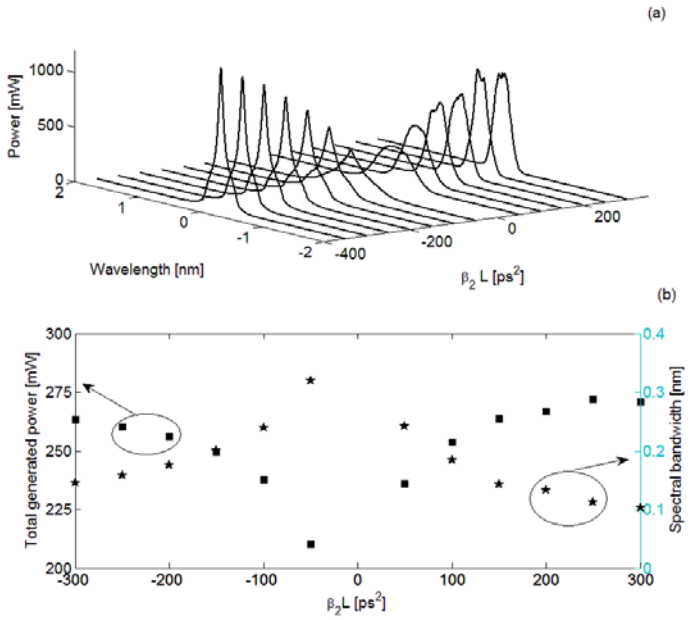

Figure N.19. a) Spectra for different $\beta_2 L$; b) Spectral bandwidth and total generated power versus $\beta_2 L$. Total pump power 700 mW.

We would like to stress that the theoretical model works rather well, for instance, Fig. N.20 demonstrates a good agreement between numerical and experimental results for the generated spectra (here the total pump power was 600 mW) [Turitsyna *et al.*, 2011].

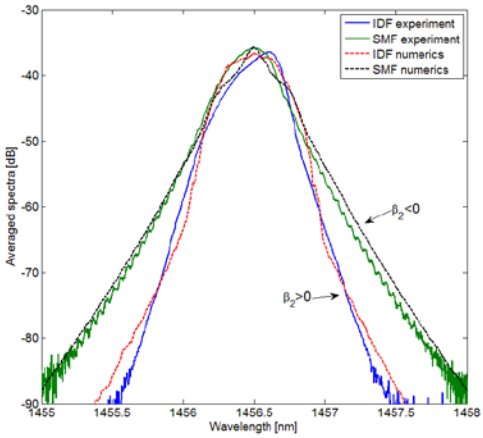

Figure N.20. Comparison of spectra of numerical simulation and experiment for SMF ($\beta 2<0$) and IDF ($\beta_2>0$) fibres with total pump power 600 mW.

N.7. Spectral condensate in fibre lasers

The evolution in the case of normal dispersion is peculiar but interesting. In the numerical simulations we considered L=22 km fibre laser and different values of pump powers (from 400 -1000 mW) and dispersion ($\beta_2 L$ in the interval [-300,300] ps^2). We have observed that in the case of an anomalous dispersion ($\beta_2<0$) generated spectra are formed and became quasi-steady after just a few round trips. In this case fluctuations in the generated power evolution are small compared to the average power level – of the order of few mW (dashed and dotted line in Fig. N.21). For the normal dispersion ($\beta_2>0$) a very narrow condensate consisting of only few modes is formed initially.

It persists for a time that depends on the number of modes and the absolute value of dispersion. During the condensate lifetime, the total intensity is constant with high accuracy (solid line in Fig. N.21, inset picture). Then the condensate experiences nonlinear instability leading to its destruction. The condensate destruction is manifested by a sharp transition to a wider spectrum and a lower mean power. That new (statistically steady) state is accompanied by strong fluctuations which seem to be a sign of bi-stability [Turitsyna *et al.*, 2009].

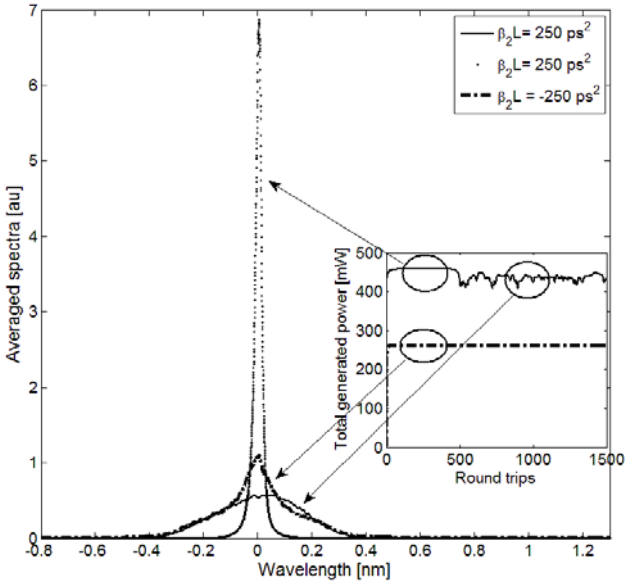

Figure N.21 Averaged spectra for normal and anomalous dispersion: solid line – normal dispersion condensate state, dotted line – normal dispersion destroyed condensate, dashed and dotted line – anomalous dispersion. Inset picture – the corresponding generated power evolution for normal and anomalous dispersions.

Fig. N.22 illustrates that the spectrum becomes broader and more top flat after about 500 round trips, with heavily oscillating tails. It reflects the intensity curve evolution in Fig. N.21 (inset picture). In the case of the opposite sign of dispersion (anomalous dispersion) we do not observe anything like this transition. In the case of anomalous dispersion the spectrum is generated from the zero noise level, then after few round trips (when the total power reaches a certain equilibrium level) it is stabilized and remains almost steady, with slightly oscillating tails (Fig. N.23). Figure N.24 characterizes fluctuations of the generated power by histograms, with the condensate distribution clearly being much narrower than both other histograms. Not surprisingly, the condensate is a less fluctuating state.

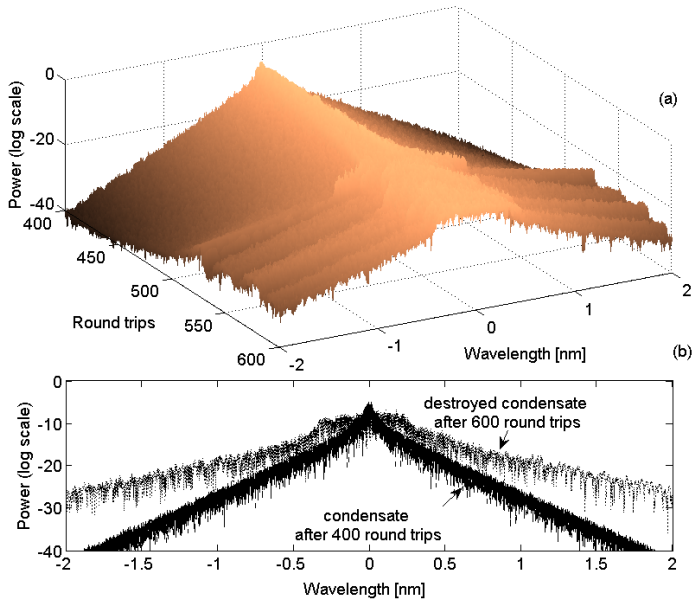

Figure N.22 a) Spectra evolution for the case with normal dispersion, when the condensate destroys after 500 round trips; b) the corresponding picture of the spectra for condensate (after 300 round trips) and after it is destroyed (after 600 roundtrips).

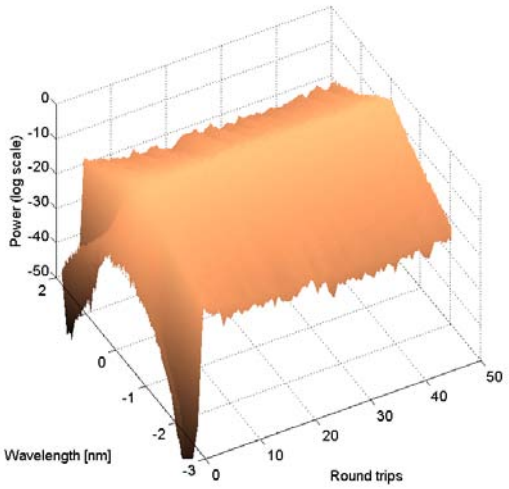

Figure N.23 Spectra evolution for anomalous dispersion.

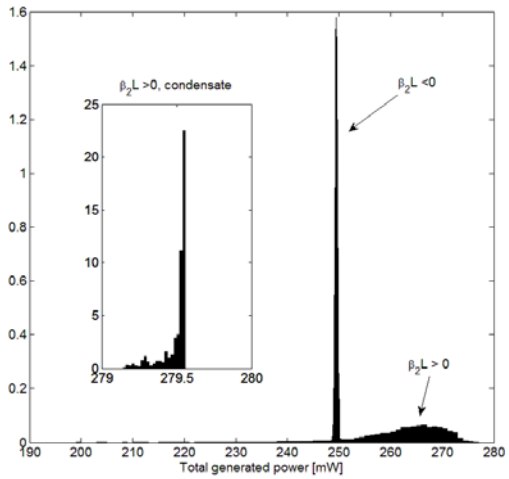

Figure N.24 Typical histogram of total generated power for normal (condensate and destroyed condensate state) and anomalous dispersion. Here $\beta_2 L = \pm 150\ ps^2$.

Note also that its histogram is very asymmetric with the highest value being most probable. It can be naturally interpreted as fluctuations being

only “dips” in the condensate such as gray and dark solitons. An abrupt decay of the probability of intensities exceeding certain value can be thought of as an interesting effect of nonlinear self-induced optical limiting. This prevents the laser power from random overshoot and might be of practical importance in power sensitive applications in laser systems providing for a stable mode condensate. On the contrary, when the condensate is destroyed, the histograms are much wider and more symmetric with substantial probability of fluctuations exceeding mean value.

Now we discuss the impact of a number of generated modes on the building of an equilibrium state. As explained in (N.3), one can estimate from this, that for FBG of 0.1 nm bandwidth (corresponds to δ_2= 277 nm^{-2}) and 800 mW of total pump power, there will be ~32,280 modes with the spectral separation between modes $\Delta=\lambda^2/(2Ln)$= $7.3\text{x}10^{-7}$ nm (here n=1.45 is a refractive index in silica). As we consider a spectral window 8 times larger than the FBG bandwidth, it gives the total number of modes used in simulations 2^{20}=1048576. Figure N.25 demonstrates the evolution of the generated spectra for fibre laser with normal dispersion cavity with this number of modes. As seen from Fig. N.25, there is no clearly pronounced condensate state for this number of modes in normal dispersion cavity.

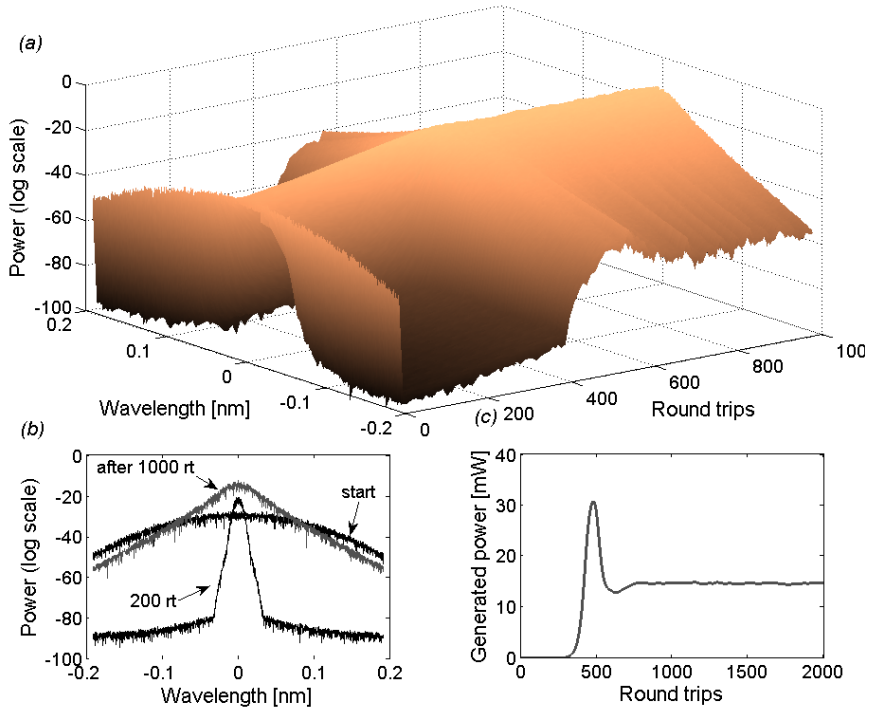

Figure N.25 Fibre laser with a cavity of 1 km long IDF fibre (normal dispersion). a) spectra evolution for the first 1000 roundtrips; b) spectra profiles on different stages – at the start, after 200 roundtrips and after 1000 roundtrips; c) evolution of the generated power.

Indeed, we have observed that the occurrence of a condensate state and properties of evolution do depend on the number of modes. For instance, Fig. N.26 shows how evolution can be drastically changed by increasing the total number of interacting modes.

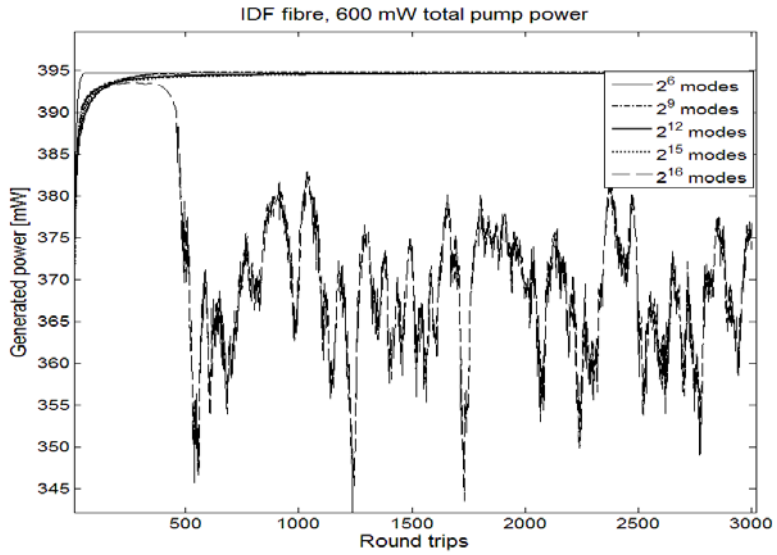

Figure N.26 Generated power evolution for different number of modes for 600 mW total pump power, 13.5 km fibre cavity length.

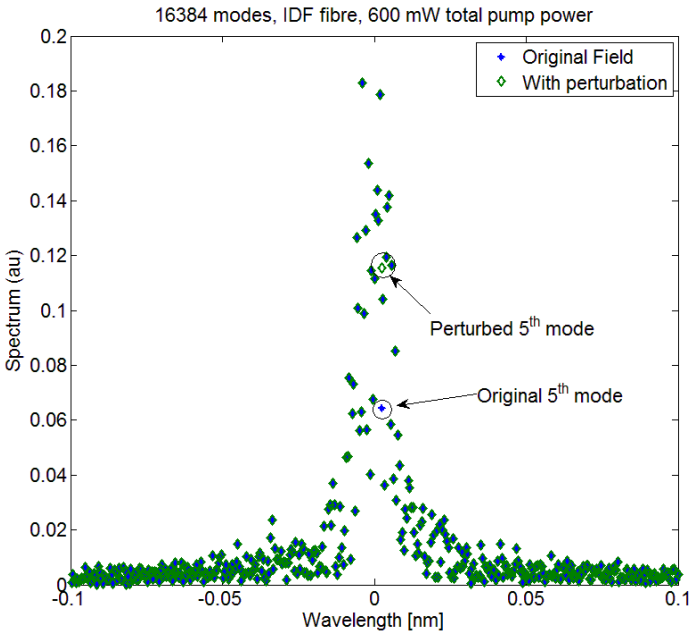

Figure N.27. Spectrum used for adding some perturbation to the 5th from the centre mode.

Transition to developed turbulence from a linearly stable condensate is an interesting problem that will be discussed in full detail elsewhere. However, we present here a brief outline showing the most important nontrivial aspects of this nonlinear problem. We have investigated how resistant the condensate state may be to small structural perturbations. We extracted the field after the initial stage when the spectra became stable in the condensate state, and then imposed a small perturbation (~10%) to the 5th (from the centre) mode (Fig. N.27). The results of these observations, the following evolution of the spectra and the generated power of the perturbed condensate state are presented in Figs. N.28-N.29.

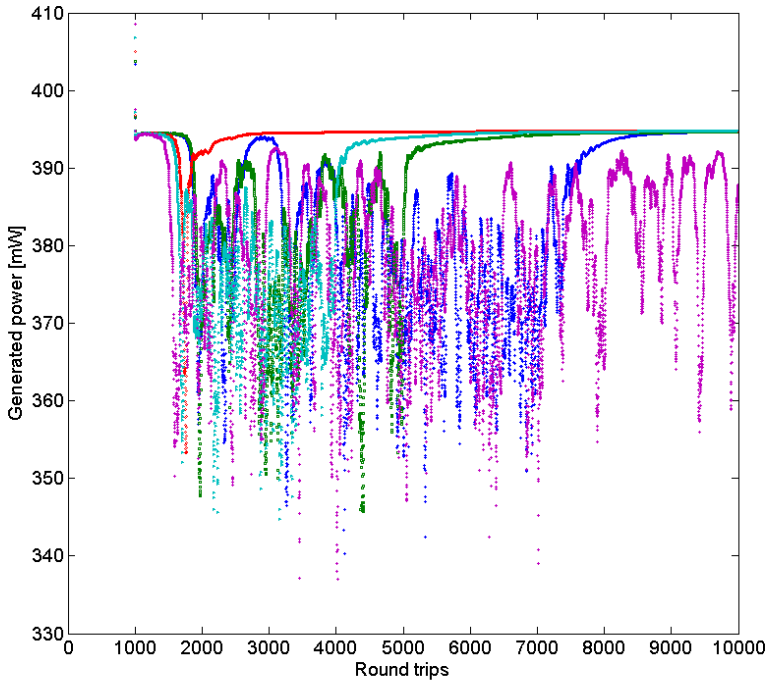

Figure N.28 Different types of intensity evolution depending on the level of perturbation.

Depending on the level of perturbation we observed (as shown in Fig. N.28) different evolutions in the generated intensity of the field: drop and recovery, non-drop and drop and not recovery. Figure N.28 illustrates

(corresponding quantitative data are given by Fig. N.29) how the initial perturbation amplitudes affect the condensate.

Figure N.29 quantifies dynamics shown in Fig. N.28 by presenting dependence of drop time and recovery time for condensate for IDF fibre, total power of 600 mW, 16384 modes, with perturbed 5^{th} mode. The generated power of the condensate state is 394.5 mW; and drop time measured at 393 mW.

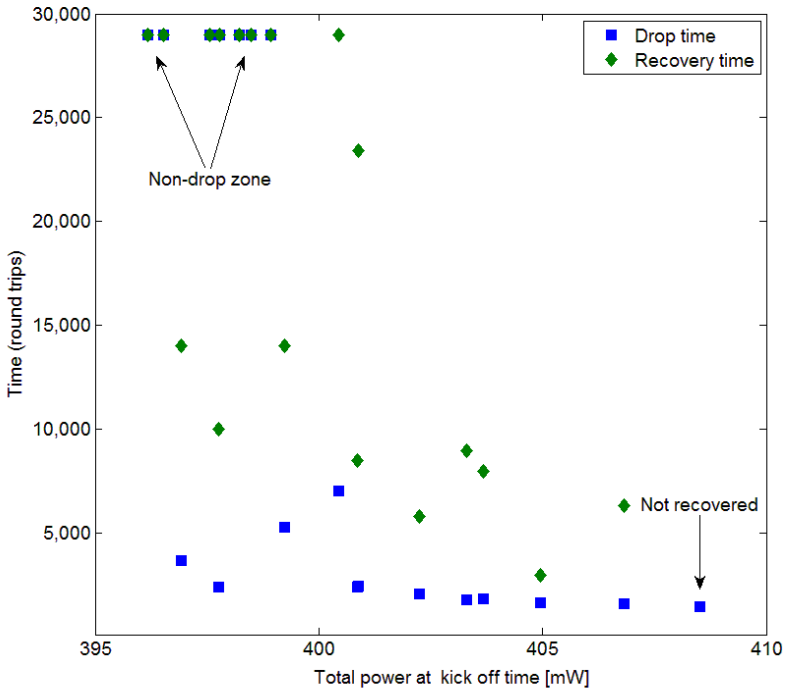

Figure N.29 Dependence of condensate's drop and recovery time on the total power at the time of perturbation.

Numerical simulations with a number of modes less than 2^{16}=65536 demonstrated a rather long existence of the condensate state. In the case of a larger number of modes the condensate state can also be observed, however, it did not last long and experienced a sharp transition to a strongly fluctuating regime. Experimental observation of the condensate

is a challenging problem and these studies will be presented in detail elsewhere.

N.8 Conclusions and perspectives

We have presented an interesting interdisciplinary link between laser science and the theory of wave turbulence. Fibre lasers can have cavity lengths ranging from a few metres to several hundred kilometres. Generated fibre laser power is distributed between multitudes of very small amplitude cavity modes. However, the resonator is not linear and the nonlinear interactions between the modes do play an important role in the operation and performance of such lasers. The spectra of generated radiation experience spectral broadening dependent on power. Thus, the nonlinear Kerr effect does affect the propagation of light in fibre lasers and leads to a nonlinear mixing of cavity modes. Any particular interaction between resonator modes can be considered as a very weak one – the properties of each wave are not changed substantially during a single interaction event. However, despite the small amplitudes of propagating waves the overall effect can be important because of the huge number of modes involved in the interactions. The efficiency of interactions depends on resonance conditions between the phases of any four participating waves – the four-wave mixing process. Even weak nonlinear interactions through the FWM process lead to a random energy transfer between waves and to an enhancement of mode de-phasing. This is because it involves a continuum of modes propagating with significant group velocity dispersion, resulting in exponential tales of the generated spectra. Note that other manifestations of the Kerr nonlinearity such as self-phase or cross-phase modulation effects might be important for overall optical field evolution, but they do not lead to the inter-mode phase difference as they change the mode phases synchronously. We stress that modes' dynamics are randomised not by noise, but due to the FWM nonlinear process that engages a huge number of deterministic interactions of rapidly oscillating modes with different amplitudes and phases making time evolution of any particular cavity mode extremely stochastic. Note that lasing is due to the Rayleigh backscattering results in a similar effect: the generation of a stochastic continuum of frequency

components. As a result the spectrum generated in random distributed feedback laser is nearly the same having a close bandwidth (~1 nm at half maximum) and similar exponential tails.

The situation with stochastic modes is somewhat similar to the classic physical problem in which long term average properties of the system are determined by a random behaviour of a huge number of weakly interacting waves (which could be of quite different physical origins) – *weak wave turbulence* [Zakharov *et al.*, 1992]. This link between the research areas of wave turbulence and laser physics also offers an opportunity to study the properties of wave turbulence in an optical device (laser) that allows very precise measurements. Note that recently such a similarity was successfully used in studies of optical rogue waves [Solli *et al*, 2007]. Our results demonstrated that the sign of cavity dispersion has a dramatic impact on optical wave turbulence that determines the spectral and temporal properties of generated radiation, directly related to the performance of fibre laser. For normal dispersion, we observe an intermediate state with an extremely narrow spectrum – spectral condensate, which experiences instability and a sharp transition to a strongly fluctuating regime. Power histograms show that normal dispersion increases the probability of a spontaneous generation of large-amplitude pulses - optical rogue waves. For anomalous dispersion, we have observed triangular spectra and more coherent temporal behaviour of the generated radiation.

Ultra-long lasers have allowed spatio-spectral transparency at long distances over a broad bandwidth even with only single-wavelength laser pumps, thanks to the extended signal gain bandwidth provided by the superposition of pump and cascading Stokes wave [Ellingham *et al.*, 2006; Ania-Castanon *et al.*, 2008]. Recent results showing simultaneous transparency over 20 nm for standard fibre links of 20 km length [Ania-Castanon *et al.*, 2008] have opened the gate to a series of novel applications, from signal processing devices, in which different channels can be made to interact nonlinearly with each other in non-dissipative

conditions, to quantum communication systems, relying on continuous quantum variables, for which these transparent links might provide an ideal medium to perform experiments on self-phase modulation squeezing of quantum optical solitons [Drummond *et al.,* 1993]. Quantum communications with transmission of a few photons are another option for which our transparent links seem to be suitable in principle, although this would, of course, require an extremely precise stabilization of the cavity characteristics, as well as of the energy of the Stokes wave trapped in the cavity. In addition, ultra-long laser cavities can be exploited in fundamentally new practical approaches for optical information transmission and secure communications. For instance, the concept of non-quantum secure key distribution based on establishing laser oscillations between the sender and receiver has been recently proposed in [Scheuer *et al*, 2006; Zadok *et al.*, 2008]. Lasers with such a large number of cavity modes interacting through wave turbulent mechanisms have never been studied before. Therefore, we believe that our results may open an entirely new research field closely linked with different areas of physics such as nonlinear science, the theory of disordered systems, wave turbulence and others. In addition to such interesting connections with many areas of fundamental science, we also anticipate that new applications and technologies will keep emerging from the study of the physics of ultra-long fibre lasers.

Acknowledgments

We would like to acknowledge valuable discussions with E.A. Kuznetsov and the financial support of the Leverhulme Trust, the Royal Society, FP7 Marie Curie project IRSES, the European Research Council, and the research grants of the Russian Federation Government N11.G34.31.0035; N11.519.11.4001 and N11.519.11.4018.

References

Agrawal, G. (1995) *Nonlinear Fibre Optics* (Academic Press, London).

Akhmediev, N, and Korneev, V. (1986) Modulation instability and periodic solutions of the nonlinear Schrö dinger equation, *Teoret. Mat. Fiz.* 69, 189–194.

Akhmediev, N., Ankiewicz, A., and Soto-Crespo, J.M. (2009). Rogue waves and rational solutions of the nonlinear Schrödinger equation, *Physical Review E*,80, 026601.

Akhmediev, N., Soto-Crespo, J.M., and Ankiewicz, A. (2009). Extreme waves that appear from nowhere: On the nature of rogue waves, *Physics Letters A*,373, pp. 2137-2145.

Ania-Castañón, J. D. (2004). Quasi-lossless transmission using second-order Raman amplification and fibre Bragg gratings, *Opt. Express*, 12, pp. 4372-4377.

Ania-Castañón, J. D., Ellingham, T.J., Ibbotson, R. , Chen, X., Zhang, L. and Turitsyn, S. K. (2006). Ultralong raman fibre lasers as virtually lossless optical media, *Phys. Rev. Lett.*,96, 023902.

Ania-Castanon, J. D., Karalekas, V., Harper, P.and Turitsyn, S. K. (2008). Simultaneous Spatial and Spectral Transparency in Ultralong Fibre Lasers,*Phys. Rev. Lett.* 101, 123903.

Aschieri, P., Garnier, J., Michel, C., Doya, V. and Picozzi, A. (2011). Condensation and thermalization of classsical optical waves in a waveguide, *Phys. Rev. A*, 83, pp. 033838.

Babin, S. A., Churkin, D. V., Podivilov, E. V. (2003) Intensity interactions in cascades of a two-stage Raman fibre laser, *Opt. Comm.*, 226, pp. 329-335.

Babin, S. A., Churkin, D. V.,Fotiadi, A.A., Kablukov, S.I., Medvedkov, O.I., Podivilov, E. V., (2005) Relative intensity noise in cascaded Raman fibrelasers,*IEEE Photon. Technol. Lett.*, 17, pp. 2553-2555.

Babin, S. A., Churkin, D. V., Ismagulov, A. E., Kablukov, S. I. and Podivilov, E. V. (2006). Spectral broadening in Raman fibre lasers, *Opt. Lett.*, 31, pp. 3007-3009.

Babin, S. A., Churkin, D. V., Ismagulov, A. E., Kablukov, S. I. and Podivilov, E. V. (2007a). FWM-induced turbulent spectral broadening in a long Raman fibre laser, *J. Opt. Soc. Am. B*, 24, pp. 1729-1738.

Babin, S. A., Karalekas, V., Harper, P., Podivilov, E.V., Mezentsev, V.K., Ania-Castañón, J.D. and Turitsyn, S.K., (2007b). Experimental demonstration of mode structure in ultralong Raman fibre lasers,*Opt. Lett.*, 32, pp. 1135-1137.

Babin, S. A., Churkin, D. V., Ismagulov, A. E., Kablukov, S. I., Podivilov, E. V. (2008a). Turbulence-induced square-root broadening of the Raman fiber laser output spectrum, *Opt. Lett.*, 33, pp.633-635.

Babin, S. A., Karalekas, V.,Podivilov, E. V.,Mezentsev, V. K., Harper, P., Ania-Castañón, J. D. and Turitsyn, S. K. (2008b). Turbulent broadening of optical spectra in ultralong Raman fibre lasers, *Phys. Rev. A*, 77, pp. 033803.

Barviau, B., Kibler, B. and Picozzi, A. (2009). Wave-turbulence approach of supercontinuum generation: Influence of self-steepening and higher-order dispersion, *Phys. Rev. A*, 79, pp. 063840.

Bernard, D., Boffetta, G., Celani,A., and Falkovich,G. (2006) Conformal invariance in two-dimensional turbulence,*Nature Physics*, 2, pp. 124-128

Bernard, D., Boffetta, G., Celani,A., and Falkovich,G.(2007) Inverse turbulent cascades and conformally invariant curves, *Phys. Rev. Lett.*, 98, 024501.

Borlaug D., Fathpour S., and Jalali B. (2009). Extreme Value Statistics in Silicon Photonics, *IEEE Photonics Journal*, 1, pp. 33-39.

Bortolozzo, U., Laurie, J, Nazarenko, S. and Residori, S. (2009). Optical wave turbulence and the condensation of light, *J. Opt Soc A*, 26, pp. 2280-2284.

Bouteiller, J.C., (2003). Spectral modeling of Raman fiber lasers, *IEEE Photon. Technol. Lett.* 15, pp. 1698-1700.

Cao, H., Xu, J. Y., Zhang, D. Z., Chang, S.-H., Ho, S. T., Seelig, E. W., Liu, X. and Chang, R. P.H. (2000). Spatial confinement of laser light in active random media. *Phys. Rev. Lett*.,84, pp. 5584–5587.

Cao, H. (2005). Review on latest developments in random lasers with coherent feedback, *J. Phys. A*,38, pp. 10497–10535.

Chabchoub, A., Hoffmann, N., and Akhmediev, N. (2011). Rogue Wave Observation in a Water Wave Tank, *Physical Review Letters*,106, 204502.

Chernikov, S. V., Zhu, Y., Taylor, J. R. and Gapontsev, V. P. (1997). Supercontinuumself-Q-switched ytterbium fibre laser,*Opt. Lett.*,22, pp. 298–300.

Chernikov, S. V., Lewis, A. E. and Taylor, J. R. (1999). 'Broadband Raman amplifiers in the spectral range of 1480-1620 nm, *Proc. Optical FibreConference*, WG6-1.

Churkin, D. V., Smirnov, S. V. and Podivilov, E. V. (2010). Statistical properties of partially coherent cw fibre lasers,*Opt. Lett.*, 35, pp. 3288-3290.

Ania-Castanon, J.D., Karalekas, V., Harper, P., and Turitsyn, S.K. (2008).Simultaneous Spatial and Spectral Transparency in Ultralong Fiber Lasers,*Phys. Rev. Lett*. 101, 123903.

Dalloz, N., Randoux, S. and Suret, P. (2010), Influence of dispersion of fibre Bragg grating mirrors on formation of optical power spectrum in Raman fibre lasers, *Opt. Lett*., 35, pp. 2505-2507.

Dianov, E. M., Grekov, M. V., Bufetov, I. A., Vasiliev, S. A., Medvedkov, O. I., Plotnichenko, V. G., Koltashev, V., Belov, A. V., Bubnov, M. M., Semjonov, S.L., Prokhorov,A.M. (1997). CW High Power 1.24 μm and 1.48 μm Raman Lasers Based on Low Loss Phosphosilicate Fibre, *Electron. Lett.*, 33, pp. 1542–1544.

DianovE.M., BufetovI.A.,Bubnov M.M., GrekovM.V.,VasilievS.A., and Medvedkov O.I.,(2000) Three-cascaded 1407-nm Raman laser based onphosphorus-doped silica fibre,*Opt. Lett.*, 25, pp. 402-404.

Drummond, P. D., Shelby, R. M. , Friberg, S. R., Yamamoto, Y. (1993). Quantum solitons in optical fibres, *Nature* 365, pp. 307 - 313.

Dudley, J. M., Genty, G., and Coen,S. (2006) Supercontinuum generation in photonic crystal fibre, *Rev. Mod. Phys*.,78, pp. 1135-1184.

Dudley,J. M., Genty, M. V., G. and Eggleton, B. J. (2008). Harnessing and control of optical rogue waves in supercontinuum generation, *Opt. Express*, 16, pp. 3644-3651.

Dudley, J.M., Genty, G., Dias, F., Kibler, B., and Akhmediev, N. (2009). Modulation instability, Akhmediev Breathers and continuous wave supercontinuum generation.,*Optics Express*,17, pp. 21497-508.

Dalloz, N., Randoux, S., and Suret, P. (2010). Influence of dispersion of fiber Bragg grating mirrors on formation of optical power spectrum in Raman fiber lasers, *Opt. Lett*. **35**, pp. 2505-2507.

Dyachenko, A., Newell, A. C., Pushkarev, A., and Zakharov, V. E. (1992). Optical turbulence: weak turbulence, condensates and collapsing filaments in the nonlinear Schrödinger equation,*Physica D*, 57, pp. 96-160.

Dyachenko, A., and Falkovich,G. (1996). Condensate turbulence in two dimensions,*Phys. Rev. E*,54, pp. 5095-5099.

Dyachenko, A.I. and Zakharov, V.E. (2011) Compact equation for gravity waves on deep water, *JETP Lett.*, 93, pp. 701-705.

Ellingham,T. J., Ania-Castañón, J. D., Ibbotson, R., Chen, X., Zhang, L. and Turitsyn, S. K. (2006). "Quasi-lossless optical links for broad-band transmission and data processing, *IEEE Photon. Technol. Lett*., 18, pp. 268-270.

Falkovich, G., Kolokolov, I., Lebedev, V.,and Migdal,A. (1996) Instantons and intermittency, *Phys. Rev. E*, 54, pp. 4896-4907.

Falkovich, G., Kolokolov,I., Lebedev,V., and Turitsyn,S. (2001) Statistics of soliton-bearing systems with additive noise,*Phys. Rev. E*, 63, pp. 025601(R).

Falkovich, G. E. (2006), *Lecture Notes on Turbulence and Coherent Structures in Fluids, Plasmas and Nonlinear Media*, v. 4, Chapter 1, "Introduction to turbulence theory," (World Scientific, Singapore) pp. 1-21.

Falkovich, G. and Sreenivasan, K.R. (2006). Lessons from hydrodynamic turbulence, *Physics Today*, 59, pp. 43–49.

Falkovsky, L.A. (2004), Investigation of semiconductors with defects using Raman scattering, *Phys. Usp*. 47, pp. 249272.

Fallert, J., Dietz, R.J.B., Sartor, J., Schneider, D., Klingshirn, C. and Kalt H. (2009). Co-existence of strongly and weakly localized random lasermodes. *Nature Photon*.,3, pp. 279–282.

Finot, C., Hammani, K., Fatome, J., Dudley, J.M., and Millot, G. (2009), Selection of Extreme Events Generated in Raman Fibre Amplifiers Through Spectral Offset Filtering, *IEEE Journal of Quantum Electronic*s,46, pp. 205-213.

Fotiadi, A. A. and Kiyan, R. V. (1998). Cooperative stimulated Brillouinand Rayleigh backscattering process in optical fibre,*Opt. Lett*.,23, pp. 1805–1807.

Fotiadi, A. A., Me´gret, P. and Blondel, M. (2004). Dynamics of a self-Q-switched fibre laserwith a Rayleigh-stimulated Brillouin scattering ring mirror,*Opt. Lett*.,29, pp. 1078–1080.

Fotiadi, A., Preda, E., and Mégret, P., (2011) Brillouin Fibre Laser with Incoherent Feedback, *Proc. CLEO: 2011 - Laser Applications to Photonic Applications*, OSA Technical Digest (CD) (Optical Society of America, 2011), paper CTuI6.

Frazao, O., Correia, C., Santos, J. L. and Baptista, J. M. (2009). Raman fibre Bragg-gratinglaser sensor with cooperative Rayleigh scattering for strain–temperaturemeasurement. *Meas. Sci. Technol*.,20, 045203.

Frisch,U. (1995) *Turbulence: The Legacy of A. N. Kolmogorov*. (Cambridge University Press).

Gottardo, S., Sapienza, R., García, P. D., Blanco, A., Wiersma, D. S. and López, C. (2008). Resonance-driven random lasing,*Nature Photon.*,2, pp. 429–432.

Grubb, S. G., Strasser, T., Cheung, W. Y., Reed, W. .A., Mizrachi, V., Erdogan, T., Lemaire, E. J., Vengsarkar, A. M. and Digiovanni, D. J. (1995). High power, 1.48 gm cascaded Raman laser in germanosilicate fibres, *Proc. Optical Amp. and their Applications*, pp. 197-199.

Hammani, K., Finot, C., Dudley, J.M., and Millot, G. (2008). Optical rogue-wave-like extreme value fluctuations in fibre Raman amplifiers, *Optics Express*, 16, pp. 16467-16474.

Hammani, K., Kibler, B., Finot, C., and Picozzi, A. (2010), Emergence of rogue waves from optical turbulence, *Physics Letters A*,374, pp. 3585-3589.

Hammani, K., Finot, C., and Millot, G., (2009). Emergence of extreme events in fibre-based parametric processes driven by a partially incoherent pump wave, *Opt. Lett.*,34, pp. 1138-1140.

Hammani, K., Picozzi, A. and Finot, C. (2011). Extreme statistics in Raman fibre amplifiers: From analytical description to experiments, *Opt. Comm*, 284, pp. 2594-2603.

Han,Y. -G., Tran, T. V. A., Kim, S. -H. and Lee, S. B. (2005). Development of a multiwavelength Raman fibre laser based on phase-shifted fibre Bragg gratings for long-distance remote-sensing applications,*Opt. Lett.*, 30, pp. 1114-1116.

Han, Y.-G., Moon, D. S., Chung, Y. and Lee, S. B. (2005). Flexibly tunable multiwavelengthRaman fibre laser based on symmetrical bending method,*Opt. Express*,13, pp. 6330–6335.

Haus, H. A. and Nakazawa, M. (1987). Theory of the fibre Raman soliton laser, *J. Opt. Soc. Am. B*, 4, pp. 652-660.

Headley, C. and Agrawal,G. (2004) *Raman Amplification in FibreOptical Communication Systems* (Academic Press, New York).

Herrmann, J. and Wilhelmi, B. (1998). Mirrorless laser action by randomly distributedfeedback in amplifying disordered media with scattering centers,*Appl. Phys. B*,66, pp. 305–312.

Hsiung, P.-L., Chen, Y., Ko, T., Fujimoto,J., de Matos, C., Popov, S., Taylor, J. and Gapontsev, V. (2004). Optical coherence tomography using a continuous-wave, high-power, Raman continuum light source,*Opt. Express*, 12, pp. 5287-5295.

Huang,S. H., Feng, Y., Shirakawa, A. and Ueda,K. (2003). Generation of 10.5 W, 1178 nm laser based on phosphosilicate Raman fibre laser, *Jpn. J. Appl. Phys.*, 42, pp. L1439-L1441.

Imam, H. (2008). Metrology: broad as a lamp, bright as a laser,*Nature Photon.*,2, pp. 26–28.

Janssen, P. A. E. M. (2003). Nonlinear Four-Wave Interactions and Freak Waves,*J. Phys. Oceanogr.*, 33, pp. 863–884.

Juarez, J. C., Maier, E. W., Kyoo, N. C. and Taylor, H. F. (2005). Distributed fibre-opticintrusion sensor systems, *J. Lightwave Technol*.,23, pp. 2081–2087.

Karpov, V., Papernyi, S.B., Ivanov, **V**., and Clements, W.R .L. (2004). Cascaded pump delivery for remotely pumpederbium doped fibre amplifiers. *Proceedings of the SUBOPTIC Conference*,We 8.8 (2004).

Kasparian, J., Béjot, P., Wolf, J.-P., and Dudley, J.M. (2009). Optical rogue wave statistics in laser filamentation" *Optics Express*, 17, pp. 12070-12075.

Kawata, T. and Inoue, H. (1978). Exact Solutions of the Derivative Nonlinear Schrödinger Equation under the Nonvanishing Conditions, *J. Phys. Soc. Jpn.*, 44, pp. 1968-1976.

Kharif, C. Pelinovsky, E and Slunyaev, A. (2009), *Rogue Waves in the Ocean*, Springer Verlag.

Kim, N. S. (2008). Review on the High-Power Pulse Fibre Laser Technology and Their Industrial Microelectronics Applications, *Rev. Laser Eng. Supplemental volume*, pp. 1115-1118.

Kivshar, Yu. S. and Agrawal, G. P. (2003) *Optical Solitons: From Fibres to Photonic Crystals (*Academic Press, New York).

Kobtsev, S., and Smirnov, S., (2005). Modelling of high-power supercontinuum generation in highly nonlinear, dispersion shifted fibres at CW pump, *Opt. Express*,13, pp. 6912.

Kolmogorov, A. N. (1941) Local structure of turbulence in an incompressible fluid at very high Reynolds numbers, *Doklady AN SSSR*, 30, 299-303.

Kuznetsov, E.A. (1977) Solitons in a parametrically unstable plasma, *Sov. Phys. Dokl.*, 22, pp. 507-508.

Lawandy, N. M., Balachandran, R. M., Gomes, A. S. L. and Sauvain, E.(1994). Laser actionin strongly scattering media. *Nature*,368, pp. 436–438.

Lega, J., Moloney J.V., and Newell, A.C. (1994). Swift-Hohenberg Equation for Lasers,*Phys.Rev. Lett*., 73, pp. 2978-2981.

Lega, J. , Moloney, J.V. and Newell, A.C. (1995). Universal description of laser dynamics near threshold, *Physica D*,83, pp. 478-498.

Letokhov, V. S. (1968). Generation of light by a scattering medium with negativeresonance absorption. *Sov. Phys. JETP*,26, pp. 835–840.

Lushnikov, P. M. and Vladimirova, N. (2010). Non-Gaussian statistics of multiple filamentation,*Opt. Lett.*, 35, pp. 1965-1967.

Ma, Yan-Chow, (1978), The complete solution of the long-wave-short-wave resonance equations, *Stud. Appl. Math.*, 59, pp. 201-221.

Markushev, V. M., Zolin, V. F. and Briskina, Ch. M. (1986). Powder laser. *Zh. Prikl.Spektrosk.*,45, pp. 847–850.

Mermelstein, M. D., Headley, C., Bouteiller, J.-C., Steinvurzel, P., Horn, C., Feder, K., Eggleton, B. J. (2001). Configurable three-wavelength Raman fibre laser for Raman amplification and dynamic gain flattening, *IEEE Photon.Techn.Lett.* 13**,** pp. 1286-1288

Michel, C., Garnier, J., Suret, P., Randoux, S. and Picozzi, A. (2011).Kinetic Description of Random Optical Waves and Anomalous Thermalization of a Nearly Integrable Wave System, *Lett. Math Phys*, 96, pp. 415-447.

Mitschke, F., Steinmeyer, G. and Schwache, A. (1996).Generation of one-dimensional optical turbulence,*Physica D*, 96, pp. 251-258

Mollenauer,,L. F., Gordon, J. P. and Islam,M. N. (1986). Soliton propagation in long fibres with periodically compensated loss, *IEEE J. Quan. Electr*. 22, pp. 157-173.

Mollenauer,,L. F., Gordon, J. P. (2006) *Solitons in Optical Fibres: Fundamentals and Application.* (Academic Press, Burlington, MA).

Mussot, A., Kudlinski, A., Kolobov, M., Louvergneaux, E., Douay, M., and Taki, M. (2009) Observation of extreme temporal events in CW-pumped supercontinuum *Optics Express*,17, pp. 17010-17015.

Nazarenko, S. (2011)*Wave Turbulence (Lecture Notes in Physics)*.(Springer-Verlag, Berlin).

Newell, A. C., Nazarenko,S., and Biven,L. (2001). Wave turbulence and intermittency,*Physica D*, 152, pp. 520-550.

Noginov, M. A. (2005) *Solid-State Random Lasers* (Springer-Verlag, Berlin).

Papernyi, S. B., Karpov, V. J. and Clements, W. R. L. (2002). Third-order cascaded Raman amplification, *Proc. Optical Fibre Conference*, FB4.

Preda, C. E., Ravet, G., Fotiadi, A. A., and Mégret, P., (2011). Iterative method for Brillouin fibre ring resonator,*Proceedings of CLEO/Europe and EQEC 2011 Conference Digest*, (Optical Society of America, 2011), paper CJ_P27.

Rayleigh Lord (Strutt, J. W.) (1899). On the transmission of light through anatmosphere containing small particles in suspension and on the origin of theblue sky. *Philos. Mag.*,47, pp. 375–384.

Randoux, S., Dalloz, N. and Suret, P. (2011). Intracavity changes in the field statistics of Raman fibre lasers, *Opt. Lett*., 36, pp. 790-792.

Ravet, G., Fotiadi, A. A., Blondel, M. and Megret, P. (2004). Passive Q-switching inall-fibre Raman laser with distributed Rayleigh feedback. *Electron. Lett.*,40, pp. 528–529.

Scheuer, J. and Yariv, A. (2006) Giant Fibre Lasers (GFL): A New Paradigm for Secure Key Distribution,*Phys. Rev. Lett*., 97, pp. 140502.

Shrira, V. I. and Geogjaev, V. V. (2007), What makes the Peregrine soliton so special as a prototype of weak waves? *J. Eng. Math.*, 67, pp. 11-22.

Skryabin, D. V., Luan, F., Knight, J.C., and Russell, P.S. (2003) Soliton self-frequency shift cancellation in photonic crystal fibres, *Science*, 301, pp. 1705-1708.

Soh, D. B. S, Koplow, J. P., Moore, S.W., et al. (2010). The effect of dispersion on spectral broadening of incoherent continuous-wave light in optical fibers, *Optics Express*, 18, pp. 22393-22405.

Solli, D. R., Ropers, C., Koonath, P. and Jalali, B. (2007).Optical rogue waves,*Nature*, 450, pp. 1054–1057.

Smirnov, S. V., Ania-Castanon, J. D., Ellingham, T. J., Kobtsev, S. M., Kukarin, S. and Turitsyn, S. K. (2006). Optical spectral broadening and supercontinuum generation in telecom applications, *Opt. Fibre Techn.*, 12, pp. 122-147.

Stolen, R. H., Ippen, E. P. and Tynes, A. R. (1972). Raman oscillation in glass opticalwaveguide. *Appl. Phys. Lett.* **20**, pp. 62–64.

Stolen, R. and Ippen, E. (1973). Raman gain in glass optical waveguides, *Appl. Phys. Lett.*, 22, pp. 276-278.

Suret, P., and Randoux, S., (2004) Influence of spectral broadening on steady characteristics of Raman fibre lasers: from experiments to questions about validity of usual models, *Opt. Comm.*, 237, pp. 201-212.

Türeci, H. E., Ge, L., Rotter, S. and Stone, A. D. (2008). Strong interactions in multimoderandom lasers,*Science*,320, pp. 643–646.

Turitsyn, S. K., Ania-Castanon, J. D., Babin, S. A., Karalekas, V., Harper, P., Churkin,D., Kablukov, S. I., El-Taher, A. E., Podivilov,E. V. and Mezentsev, V. K., (2009). 270-km Ultralong Raman Fibre Laser,*Phys. Rev. Lett.* 103, 133901.

Turitsyn, S. K., J. D., Babin, S. A., El-Taher, A. E., Harper, P., Churkin,D., Kablukov, S. I., Ania-Castanon, Karalekas, V., J. D., Podivilov, E. V., (2010). Random distributed feedback fibre laser,*Nature Photonics*, 4, pp. 231-235.

Turitsyn, S.K., Bednyakova, A.E., Fedoruk, M.P., Latkin, A.I., Fotiadi, A.A., Kurkov, A.S., and Sholokhov, E., (2011). Modeling of CW Yb-doped fibre lasers with highly nonlinear cavity dynamics, *Optics Express*,19, pp. 1227-1230.

Turitsyna, E. G., Falkovich, G, Mezentsev, S. K. and Turitsyn, S. K., (2009). Optical turbulence and spectral condensate in long-fibre lasers, *Phys. Rev. A*, 80, 031804(R)

Turitsyna, E. G., Turitsyn, S. K. and Mezentsev, V. K. (2010), Numerical investigation of the impact of reflectors on spectral performance of Ramanfibre laser, *Optics Express*, 18, pp. 4469-4477.

Turitsyna, E. G., Falkovich, G., El-Taher, A., Harper, P., Shu, X., and Turitsyn, S. K. (2011) Optical turbulence and spectral condensate in fibre lasers, *Proc. IQEC/CLEO Pacific Rim 2011*.

Trulsen, K. and Dysthe, K. B. (1997). Freak waves- A three-dimensional wave simulation, Proc. 21st Symposium of Naval Hydrodynamics, pp. 550-560.

Vasilyev, M. (2003) Raman-assisted transmission: toward ideal distributed amplification, *Proc. Optical Fibre Conference*, pp. 303.

Vergeles, S. and Turitsyn, S.K. (2011) Optical rogue waves in telecommunication data streams,*Phys. Rev. A*, A 83, 061801(R).

Wang, Y. and Po, H. (2003) Impact of cavity losses on cw Raman fibre lasers, *Opt. Eng.*, 42, pp. 2872-2879.

Wiersma, D. S. and Cavalieri, S. (2001) A temperature tunable random laser. *Nature,*414, pp. 708–709.

Wiersma, D. S. (2008). The physics and applications of random lasers,*Nature Phys.*,4, pp. 359–367.

Wiersma, D. S. (2009). Laser physics: random lasers explained? *Nature Photon*. **3**, pp. 246–248.

Zadok, A., Scheuer, J., Sendowski, J. and Yariv, A., (2008) Secure key generation using an ultra-long fibre laser: transient analysis and experiment, *Opt. Express* 16, pp. 16680-16690.

Zakharov, V. E., L'vov, V. S. and Falkovich, G. (1992) *Kolmogorov Spectra of Turbulence, (*Springer-Verlag, Berlin).

Zakharov, V., Dias, F. and Pushkarev, A. (2004). One-dimensional wave turbulence, *Physics Reports*, 398, pp. 1–65.

Zakharov, V., and Nazarenko, S. (2005) Dynamics of the Bose-Einstein condensation, *Physica D*, 201, pp. 203-211.

Zakharov, V. E. and Gelash, A. A. (2011), Solitons on unstable condensate, *arxiv.org: 1109.0620v2*